Investigation of thermo-mechanical shape memory signatures of 3D printed and Injection molded polymers

Ijaz Akbar, Mourad El Hadrouz, Mohamed El Mansori, Mostapha Tarfaoui

Investigation of thermo-mechanical shape memory signatures of 3D printed and Injection molded polymers

Ijaz Akbar[a], Mourad El HADROUZ[a], Mohamed El MANSORI[b,c], Mostapha TARFAOUI[d]

[a]Arts et Metiers Institute of Technology, MSMP, HESAM Université, F-51006, Châlons-en-Champagne, France.
[b]Arts et Metiers Institute of Technology, MSMP, HESAM Université, F-13617 Aix-en-Provence, France.
[c]Texas A&M Engineering Experiment Station, College Station, TX 77843, USA.
[d]École nationale supérieure de techniques avancées (ENSTA) Bretagne, 29200 Brest, France

Corresponding author. Email contact: ijaz.akbar@ensam.eu

Abstract

This research paper investigates the shape memory signatures (SMSs) of SMPs fabricated by two different manufacturing processes, namely Fused Filament Fabricated (FFF) and Injection-molding (IM). The SMSs of each manufacturing route is first investigated by rating the thermophysical and thermodynamic properties of amorphous and semicrystalline-type shape memory polymers. Secondly, the capturing of SMSs is completed by a series of thermomechanical shape programming/recovery cycles on FFF printed specimens, and the results are correlated with the IM-produced samples of similar nature. Furthermore, the thermomechanical cycles are programmed at varying heating rates (1, 2, 3, and 5 °C.min^{-1}) to analyze their influence on shape memory behavior and cycling time. Results depict that an increase in induced pre-strain driven by small to large deformations (10% → 25%) in the elastic range leads to maximum shape memory performance and the highest performance was reported while heating at 2 and 3 °C.min^{-1}, respectively. Finally, the IM-produced samples showed slightly better shape recovery compared to the 3D-printed samples. The shape memory signatures of 3DP specimens are indeed up to 86 % like the ones produced by injection molding, which is mostly governed by the distinct residual stress/strain induced during the two different manufacturing processes.

Keywords: 3D/4D printing; Injection molding; shape memory polymers; shape memory signatures; Thermomechanical characterization; Shape programming

1. Introduction

Additive manufacturing (AM) opened new perspectives to produce complex geometries withholding advanced properties and functionalities. AM or 3D printing has minimized the part design and fabrication limitations, mainly those experienced with conventional manufacturing and plastic production promising approach called injection molding [1]. 3D printing (3DP), especially Fused Filament Fabrication (FFF) and Injection Molding (IM) both employed to fabricate the polymeric components [2]. Whereas FFF additively deposes the layer-upon-layer to complete the part, and in the IM process the molten plastic is injected with high pressure into a metal mold through an injection gate to fabricate highly dense parts [3,4]. 3D printing is a reality now to boost industrial production. Meanwhile, to get tight tolerances and high-speed repeatability, industrial production-level 3D printers are potentially expensive [5].

AM and IM-produced parts are mainly the subjects of interest in many studies, focusing largely on improving their mechanical properties in response to tunned process parameters [6,7]. The ultimate tensile stress of 3DP and IM-produced specimens concerning the printing process, printing materials and tensile testing at room temperature are evident in Fig. 1. Results indicate, overall, the IM specimens resist better than 3D-printed specimens however, the objective here is to discuss the final effects on shape memory properties rather than proving that one is better than the other. Podsiadły et al. [6] compared the mechanical properties (tensile strength) of FFF-printed and IM-produced ABS specimens of a similar nature. They found the IM parts were relatively dense due to high-pressure cavity filling, and consequently, the formation of crystalline structures helped to gain better mechanical properties than the FFF process. Another study reported by Franchetti and Kress. [8] discussed in detail the cost break-even points for 200 units based on batch size, weight, density, energy used, labor, and machine cost. Overall results came in favor of IM based on production cost and cycle time, irrespectively FFF stayed superior in the case of producing intricate parts, upfront cost, and rapid customization (Table 1). Haq et al. [7] prepared the samples with both technologies using composites of PCL/PLA and compared the results, such as impact and tensile strength, elastic and flexural modulus, respectively. They noticed that the tensile strength and elastic modulus of FFF-produced samples accounted for 65.13% and 51.76% of IM-produced parts. In addition, similar tendencies were reported for flexural and impact strength. However, they did not mention the crucial printing parameters of FFF printed parts, such as infill percentage, printing orientation, etc. Meanwhile, the deliberate choice of printing and process parameters recommended by Akbar et al. [9] for FFF-printed samples have triggered the ultimate tensile stress of SMPs up to 90% (SMPJ-3DP) of injection-molded specimens (Fig. 1). Zhao et al. [10] analyzed the tensile strength and young's modulus of FFF-printed ASTM dogbone PLA specimens at varying layer heights and printing orientations. They reported a maximum tensile strength of 49.66 MPa at 90° printing orientation with 0.1 mm layer height. Similarly, a minimum value of 19.16 MPa has been reported while they selected a maximum layer height of 0.3 mm and a minimum orientation angle of 0°.

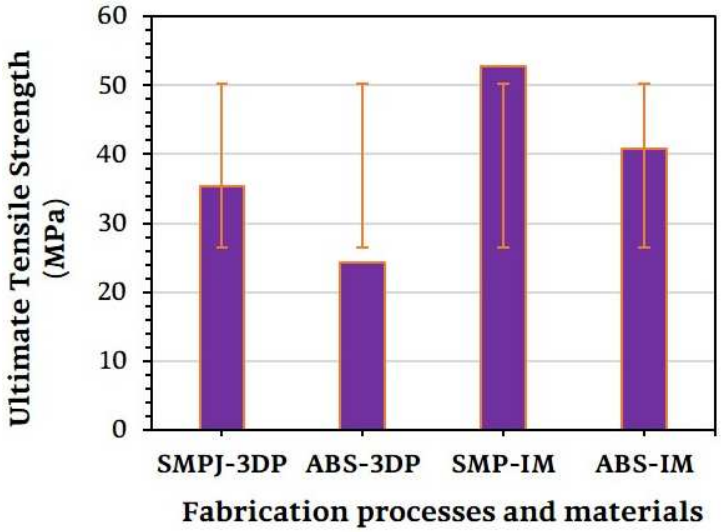

Fig. 1. Comparison of mechanical behavior of 3D printed and Injection molded specimens.

Components produced by injection molding have higher density, surface finish, tight tolerance, and short cycle time than FFF. On the other hand, the capital cost is very high and needs a longer duration to come into practice [2]. Although, current 3D printing techniques are limited to a maximum deposition rate of 50 $cm^3.hr^{-1}$ and an operation rate of 10 $mm^3.\ hr^{-1}$ [11]. Fig. 2 illustrates the principal dissimilar factors of both technologies. In addition, Table 1 exemplifies the remarks on both manufacturing processes, especially, based on the crucial need for shape memory signatures (SMSs) under shape programming/recovery for two-way (2W) and multiple-way SMPs. Therefore, how the thermomechanical cycles could affect the shape memory properties during shape programming and recovery cycles needs full-field characterization of the material to effectively define the repetitive behavior of the functional structures. Those structures can possess exciting applications for 4D printing. Whereas 4DP is the transformation of 3D-printed shape-memory-based structures into a new form (4^{th} dimension) through a thermomechanical cycle [4].

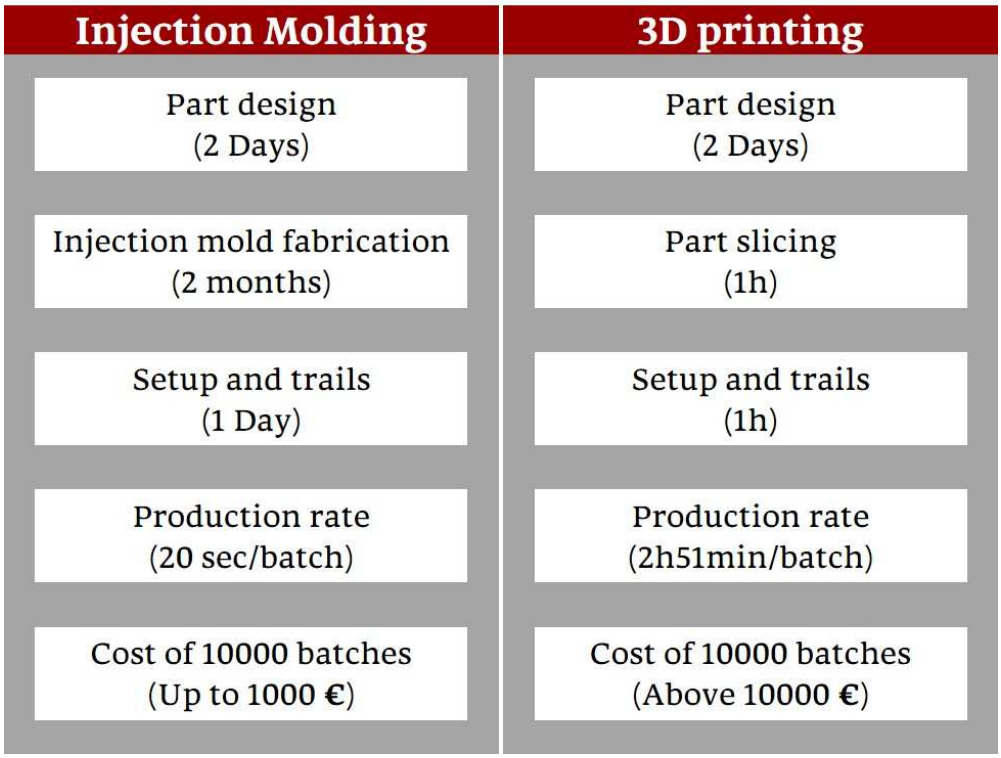

Fig. 2. General correlation of injection molding and 3D printing processes [2].

Table 1. Shape memory effects, affected by their production processes.

Injection molding (IM)	3D printing (AM)	Possible influence on SMSs	Ref.
Part properties are limited to being tunned	Higher possibility to tune the parts properties	Tunned property parts are prone to better shape memory effects, especially for ordered actuation	[4]
Higher use of material and unmanaged porosity %	Lower utilization of material even at 100% infill density and a manageable porosity %	The controlled matrix porosity can enable 2W and multiple-way SMSs, which is possible in the case of AM than in IM	[12]
Uncontrolled orientation of molecular chains	Multiple orientation-based 3DP can enable controlled molecular chains	Structured molecular chains could enable controlled actuation and recovery behavior	[3,13]
Difficult to produce and remove intricate parts	3D printing came to mitigate this issue	Complex cellular type structures are prone to higher SMS effects, thus easy to produce by AM	[7]
Homogeneous strain storage and release	Heterogeneous strain storage/release, higher in the bottom layers than a top	Faster release of stored strain to perform quick recovery in case of IM than 3DP	[6,14]

Ultimately, rather than significant gaps in mechanical properties discussed over both manufacturing processes, the primary focus of this study is to investigate the throughput of shape-memory signatures (SMSs) considering shape programming and recovery performance while subjected to two different fabrication processes under a unique specimen type and thermomechanical cycling conditions. The layer-upon-layer deposition in the FFF process causes imbalance heat transfer from the base layer towards subsequent layers, which induces a pre-strain (responsible to SMSs) in the descending direction means a higher pre-strain in the bottom layer than in the top [14]. Although, the mold filling process in the case of IM is more uniform and does not contain heterogeneous pre-strain values. Therefore, how the fabrication process variability will affect the SMSs is discussed in this work, and according to the best of our know-how there is no existing research that correlated such findings of SMPs produced by AM and IM processes.

To this end, the framework of this study includes the precise characterization of two SMPs for their thermophysical and thermodynamic properties used to predict the thermo-responsive shape programming temperatures i.e., the glass transition temperature T_g, maximum end recovery temperature (higher temperature (T_h) then T_g), specific heat capacity, and polymer weight reduction as a function of the temperature of two different SMP materials. Secondly, the variations in shape memory effects by FFF-produced parts at different heating rates are also yet not reported [15,16]. Therefore, the particular heating rates (1,2,3, and 5 °C.min^{-1}) for shape programming/recovery that primarily introduce different programmable strains, recovery time, and simultaneously affect the shape recovery ratios, is discussed and compared with injection molding results. In addition, the microscopic level thermomechanical shape memory tests were performed using a precisely controlled environment chamber equipped with an advanced video extensometer (AVE-2), however, the majority of the existing studies mainly performed the shape memory tests using macroscopic level methods i.e., shape programming/recovery in a hot water bath without using a stable environment and monitoring instruments to capture the time-temperature strain, temperature-dependent recovery time, recovery stress, shape recovery, and fixity ratios, respectively [17–20]. Finally, further investigations also highlighted whether the shape recovery behavior responded better at around 10% (small deformation) or 25% (large deformation) during extension-recovery analysis. The shape memory properties resulting from 3DP and one molded by the injection process are expected to be agreeable qualitatively and quantitatively with each other.

2. Materials and Experimental Methods

2.1 Material and methods

2.1.1 SMP materials for FFF

Two well-known and easily available SMPs are characterized in this study for the researcher community looking for intelligent materials and their properties to enable 4D printing of self-morphing structures. The discussed SMPs are missing their thermodynamic and thermophysical properties to activate their shape memorability to perform multiple programming and recovery cycles. Therefore, the need for analytical computations was indispensable. The first filament was provided by SMP Technologies Co., Ltd (Japan) with a regular Ø1.75 mm for a FFF 3D printer. This material is a thermoplastic shape memory polyurethane whose network or net points are linked with more than two chains and the microscopic phases corresponding to hard segments to enable better shape recoverability [21].

The second filament notably "eSUN 4D filament" was manufactured by Shenzhen eSun Industrial Co., Ltd (China), which is a commercial PLA-type SMP. To uniquely discuss the shape memory properties of both SMPs, the SMP bought from Japan is named SMPJ, and the other bought from China is named SMPC. Currently, PLA is the top consumed 3D printing filament however, SMPC-type PLA-based material has not been yet investigated for 4D printing and its shape memorability. Meanwhile, the 3D/4D printing and applications of SMPJ polymer were mainly discussed in several publications. Therefore, for the 3D printed sample's thermomechanical programming/recovery experiments, a thermoplastic-type amorphous SMPJ filament was selected. This SMP is a broadly discussed shape memory polymer withholding up to 400% recoverable strain properties to enable 4D printed structures and applications [9,21–23].

Both materials are pure SMPs without holding reinforced composition and belong to dual-type shape memory behaviors that can switch between one temporary and one permanent shape. Zeng et al. [24] reported rather than pure SMP, short fiber reinforced SMP possesses better deformation for shape programming and has shown slight improvements in SMS properties/recoveries. However, the shape transition process is seen more smooth in pure SMP than in increased fiber-reinforced SMPs. Since the molecule’s network structures are responsible to memorize the permanent shape of the object hence, the selected SMP’s networks are composed of hard and soft segments (usually polyols). Therefore, both SMPs have single shape fixing and single shape recovery states, then two shape recovery steps in the case of 2 way SMPs. The basic thermal and mechanical properties of both polymers are illustrated in Table 2.

Table 2. Basic properties of both SMP filaments

Description	SMPC	SMPJ
Printing temperature (°C)	200~230	195~225
Plateau Temperature (°C)	35~50	40~55
Transition temperature (°C)	45~90	45~75 [25]
Printing speed (mm/s)	40~90	30~65 [9]
Tensile strength (MPa)	58	25~36 [23]
Density (Kg.m^{-3})	1230	1147 [9]
Filament diameter (mm)	1.75	1.75
Shape recovery response (%)	95	90~99 [23]
Strain rate (%)	N/A	≥ 400 [26]

2.1.2 3DP of specimen for shape programming

Because of the comparative nature of this study, an identical specimen to the injection molding process was fabricated using a FFF 3D printer according to ASTM D638-14 Standard Test Method for Tensile Properties of Plastics [27]. In this context, a D638 Type-I specimen of length 165 mm, an overall gauge length of 57 mm, a width, and a cross-sectional area of 13 x 3.2 mm was designed, sliced, and fabricated (Fig. 4) using a precise Volumic Ultra 3D printer. The FFF printer holds x/y precision of 15 microns, z precision of around 1 micron, and printing resolution of 1-275 microns, respectively. The predefined printing parameters used to slice the model in Simplify3D software are compiled in Table 3. From the two discussed SMPs in the last section (SMPC and SMPJ), the characterization results have proven the SMPJ properties are more relevant to correlate the SMS behavior of FFF and IM-produced specimens. Therefore, the 3D-printed specimens for shape programming and recovery tests are only produced using the SMPJ material. Similarly, the following sections containing thermomechanical shape programming/recovery are solely related to SMPJ polymer. The successful printing practices to print low glass transition SMP are reported in our previous work, and similar pre-printing considerations were adopted to print SMPJ specimens [9]. The detailed fabrication process of the injection-molded SMP samples that are confronted with the FFF printed specimen in this study can be seen elsewhere [28,29].

Table 3. Printing parameters to print samples for shape memory testing's

Description	SMPJ
Printing temperature (°C)	220
Bed temperature (°C)	45
Layer thickness (mm)	0.2
Printing speed (mm/s)	40
Infill density (%)	100
Perimeters	3
Filament diameter (mm)	1.75
Nozzle diameter (mm)	0.6
Top/bottom solid layers	3
Raster orientation	90/0°
Printing orientation	Flat

2.2 Experimental tools and techniques

Shape memory programming is a complex, timely, and costly thermo-mechanical process to determine the printed structure's reversible performance. Currently, the customized shape transformation and recovery of complex objects is a challenging task [4]. Shape programming or material programming demonstrates the post-processing functionality of 3D printed structures to transform into 4D printing. At specific stimuli, the cell's movements are encoded into a physical material/structure to store or release the strain energy to enable dynamic functionalities. Similar to the programmability of natural materials and objects such as the carnivorous plant Dionaea, man-made functionally graded materials can also be programmed for 4D printing employing different stimuli [30]. Akbar et al. [4] discussed several shape programming stimuli such as thermo-responsive, light-responsive, moisture-responsive, and electro-magneto-responsive types to enable reversible SMS properties. SMPJ samples investigated in this study are prone to thermo-responsive shape memory effects which could be activated within hot water, through direct sun energy, and inside the environmental chamber. The present study performed the thermomechanical SMP tests mainly using a quasi-static loading for shape programming and zero stress recovery upon heating above T_g.

Aberoumand et al. [14] used a Programmable Logic Controller heating cooling liquid chamber with a 3-point bending fixture for shape programming. Zhao et al. [20] investigated the SMS properties of stereolithography-printed polyurethane acrylate-based SMP using a hot water bath for shape programming/recovery. They analyzed the shape recovery at different temperatures of 75, 85, and 90 °C in a hot water bath and reported at a higher temperature the recovery took 8.5 s as compared to 18 s at 75 °C. Rather than shape programming and recovery stimulus discussed above, Tiwari et al. [31] reported the shape recovery of the additively manufactured 3D smart surfaces through reverse engineering. The samples were scanned, and the cloud point data helped to generate the CAD geometry of the recovered object to compare with the real one. However, to account for accurate enough data, continuous programming, cooling to fixity, unloading, and reheating for a smooth shape recovery, a controlled environment is needed [27,28].

2.2.1 SMP's experimental characterization

To achieve precise characterization performance, differential scanning calorimetry (DSC) and dynamic mechanical analyzers (DMA) are recommended as superior solutions [23,32,33]. A DSC analyzer was employed to characterize the thermodynamic natures of two SMPs: SMPC and SMPJ, especially the glass transition, crystallization, and melting temperatures of the selected polymers. Glass transition temperature (T_g) is a crucial factor in potentially defining and exercising the thermomechanical shape programming/recovery tests. In this context, three samples of both materials weighted 13.0 mg, 15.3 mg, and 21.57 mg for SMPC, 14.3 mg, 14.4 mg, and 21.92 mg for SMPJ were tested on a NETZSCH DSC 214 instrument. The first two experiments were conducted at 10 °C.min^{-1} on both materials, and the third experiment at 1 °C.min^{-1} for heating-cooling until 250 °C to 0 °C. In addition, the DSC results including the temperature-dependent specific heat capacity are discussed in the results section.

2.2.2 Experimental setup for SMSs cycle

An environmental chamber with a controlled temperature programming facility is the current most reliable resource for specimen heating for shape programming and recovery to address 4D printing. In this regard, similar to an environmental chamber used for injection molded specimen testing [29], the equipment used in this study has a similar setup with a complete INSTRON® load frame setup as presented in Fig. 3 that was used to perform the precise thermomechanical testing and record the required SMS information. The environmental chamber belongs to INSTRON® 0007247 series with a forced convection heating and cooling distribution for precise thermal stability. A proportional integral derivative (PID) industrial regulator advanced the possibility to control and define the temperature cycle. The cooling cycle was regulated while installing a cooling valve between the environmental chamber and the self-pressurizing liquid nitrogen tank as marked in Fig. 3.

A contacting type extensometer can generate inaccurate data due to the inertia of the dynamic parts. Although, the strain rate in the present case is low enough to neglect dynamic effects. In addition, due to the limited elastic modulus of SMPs above T_g, the traditional contacting extensometer might influence the structure's dimensional stability and precision of the measured strains. Thereby, it's recommended to use a non-contacting high-resolution digital camera-based, real-time Digital Image Correlation (DIC) system named Advanced Video Extensometer (AVE-2), especially, for SMPs thermomechanical cycles as shown in Fig. 3. AVE-2 by INSTRON® setup allowed to measure the errorless strain values at higher temperatures during loading for extension, during unloading for shape fixity values, and during reheating to measure the stress-free shape recovery ratios, individually. The AEV-2 instrument belongs to the INSTRON® 2663-901 family that can be suitable to use under variable heating-cooling rates and copping testing standards of ASTM D638 and ISO 527 [35].

Overall, due to the comparative study, similar experimental procedures were adapted for the 3D printed specimen to their counterpart injection molded to provide maximum correlation from the experimental point of view and discuss the differences due to the fabrication process. For example, similar protocols include environmental chamber, thermal and mechanical boundary conditions, sample preparation for shape memory cycle, sample material, geometry, and dimensions. However, the only different equipment was the deformation recording/measurement system, for injection molded specimens, they used a vision image correlation 3D (VIC-3D) system [29], and in 3D printing, we used an advanced video extensometer, although both are working on the same principle of image correlation.

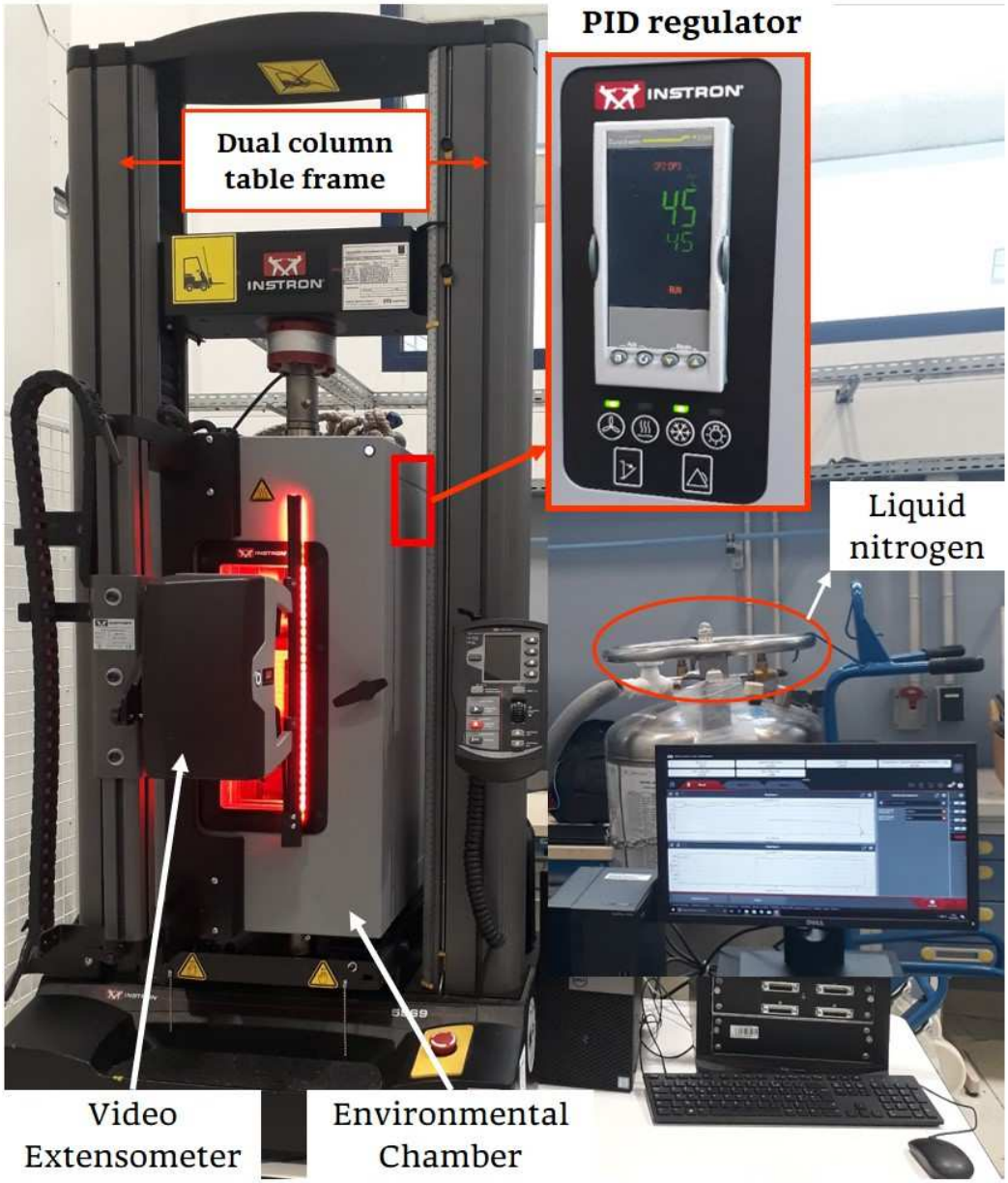

Fig. 3. Experimental setup used to perform thermomechanical shape memory cycle on FFF printed SMPJ specimens.

2.2.3 Sample preparation for SMSs cycle

As highlighted in Fig. 4, the ASTM D638 Type 1 sample was prepared with two longitudinal and transverse reference configuration dots on the gauge length. The gauge region (black highlighted area) is considered for measuring strain properties and shape programming factors such as extension/strain and recovery ratios. The initial distance between the grippers is set at 115 mm labeled as (L), and single side gripping area (Ga) was 25 mm. Considering the same constraints such as material class and sample dimensions, the gauge length of the ASTM Type-1 dog bone specimen will be extended by 10% and 25%. Initially, a non-contacting video extensometer captured and stored the reference configuration points (the highlighted white points inside the red rectangular shapes) to precisely measure the resulting outcomes concerning final configurations. At this stage, the specimen was kept stress and temperature free to ensure no thermomechanical effects. Importantly, the nominal strain values in this study are measured from the change in the length divided by the initial value of the gauge length.

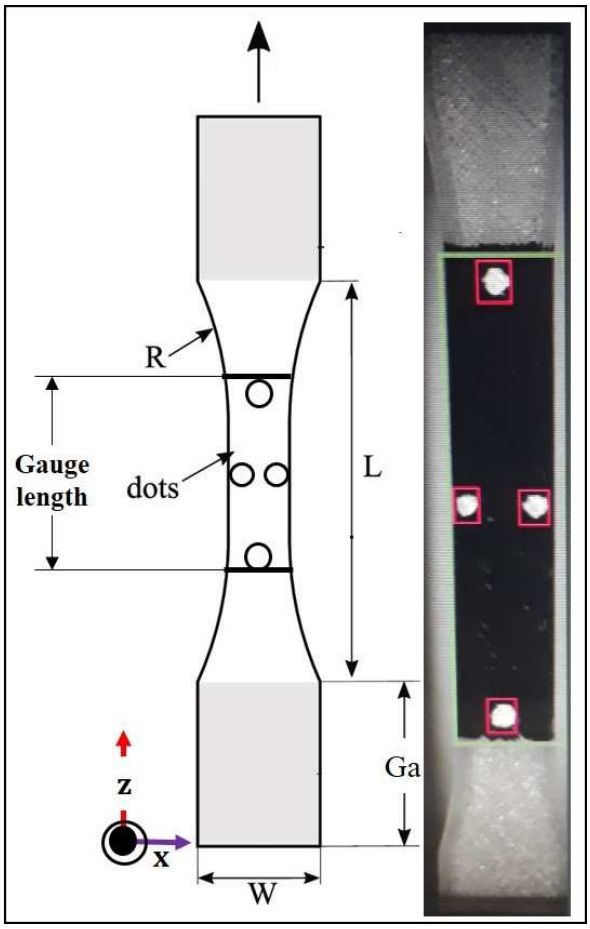

Fig. 4. 3D printed shape memory polymer (SMPJ) specimen definition and preparation for thermomechanical shape programming cycles.

2.2.4 Thermomechanical conditions for SMSs cycle

The aim to perform thermomechanical cycles on the selected SMPJ sample is to study their shape memory effects variation under different extension and similar experimental conditions. Fig. 5 illustrates the typical thermomechanical cycle of thermal-induced SMPJ to successfully conduct the shape programming as-well-as recovery tests. The boom and bust of Fig. 5 following a single heating-cooling cycle at 3 °C min^{-1} are defined as follows;

- A → B: The sample was fixed from the gripping area and kept stress free during heating from 20 °C to $T_g + 10℃$ (60 °C) at a rate of 3 °C.min^{-1} following a thermal stability delay of 120s, the similar thermal equilibrium times between 2 min and 5 min were implemented by Aberoumand et al. [14] and Choong et al. [11], respectively.
- B → C: shape programming (loading) according to defined 10 or 25 % of applied extension/strain at a steady temperature and the applied strain maintained for 2 min for further stability before cooling.
- C → D: cooling to 20 °C at 3 °C.min^{-1} to fix the programmed shape, a property of SMP materials. The stored programmed shape at a glassy state and physical aging during this shape fixity (especially for amorphous polymers) can affect the shape recovery ratios, therefore, a well-defined thermomechanical cycle is indispensable [34].
- D → E: unloading at a constant 20 °C and providing the thermal stability for another 120s to measure the stress-free shape fixity in relation to object dimensions just before unloading.
- E → F: reheating to $T_g + 20$ ℃ (70 °C) withholding 120s isothermal delay to ensure the full release of residual strains to enable the maximum shape recovery and measure the stress-free strain recovery ratios, findings of heating for programming and reheating for recovery at 10 °C higher than programming can be seen elsewhere [14]. In addition, Wang et al. [35] and Li et al. [36] reported higher shape recovery properties while selecting an end recovery temperature of T_g+15 °C, respectively. Xiao, [34] discovered the programming temperature is the base to select an appropriate end recovery temperature and is usually noticed as higher than the programming one.
- F → G: finally cooled to 20 °C to maintain the recovered shape and end the first thermomechanical cycle.

From the given heating history evaluation diagram, the reheating stage for shape recovery is devoted to the stress-free release of stored strain energy to regenerate the initial form of the object [37].

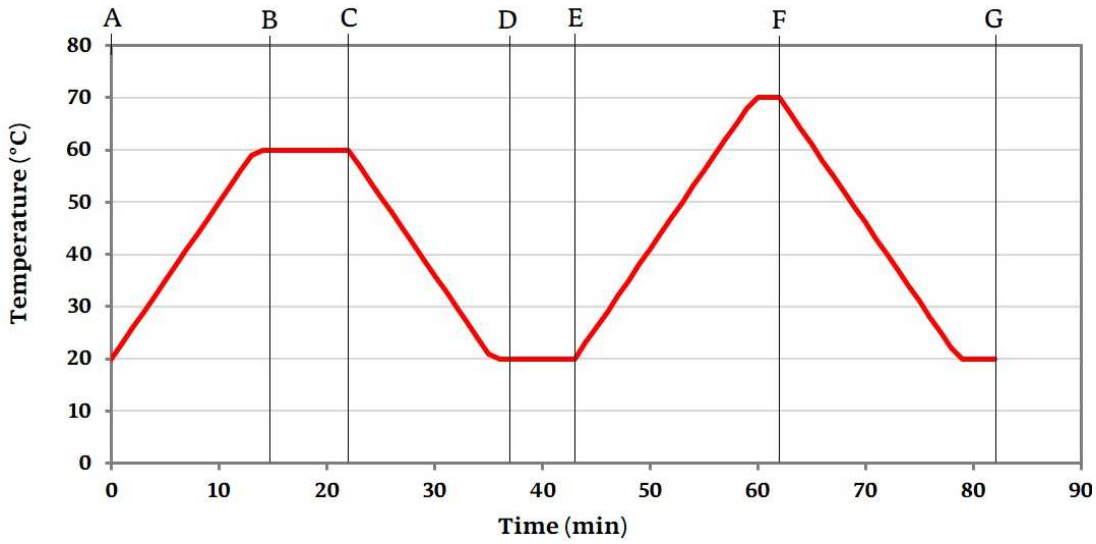

Fig. 5. Thermomechanical shape memory cycle description at 3 °C.min^{-1}.

Furthermore, Fig. 6 present the samples with boundary conditions and their further proceeding to complete the thermomechanical cycle. Initially, at room temperature, the sample is fixed according to ASTM standard method for the D638 specimen from both sides [27], and the reference configuration is highlighted by fixed white dashed lines (Fig. 6b). Secondly, the sample was heated to the above T_g and extended to 10 % or 25 % in tensile mode, according to predefined analytical requirements. In addition, the unloading step involves the release of the bottom gripper to free the specimen as prescribed in the comparative IM sample study [29], and finally, reheating above T_g enables stress-free recovery. The physical replica of the performed thermomechanical cycle is shown in Fig. 6b.

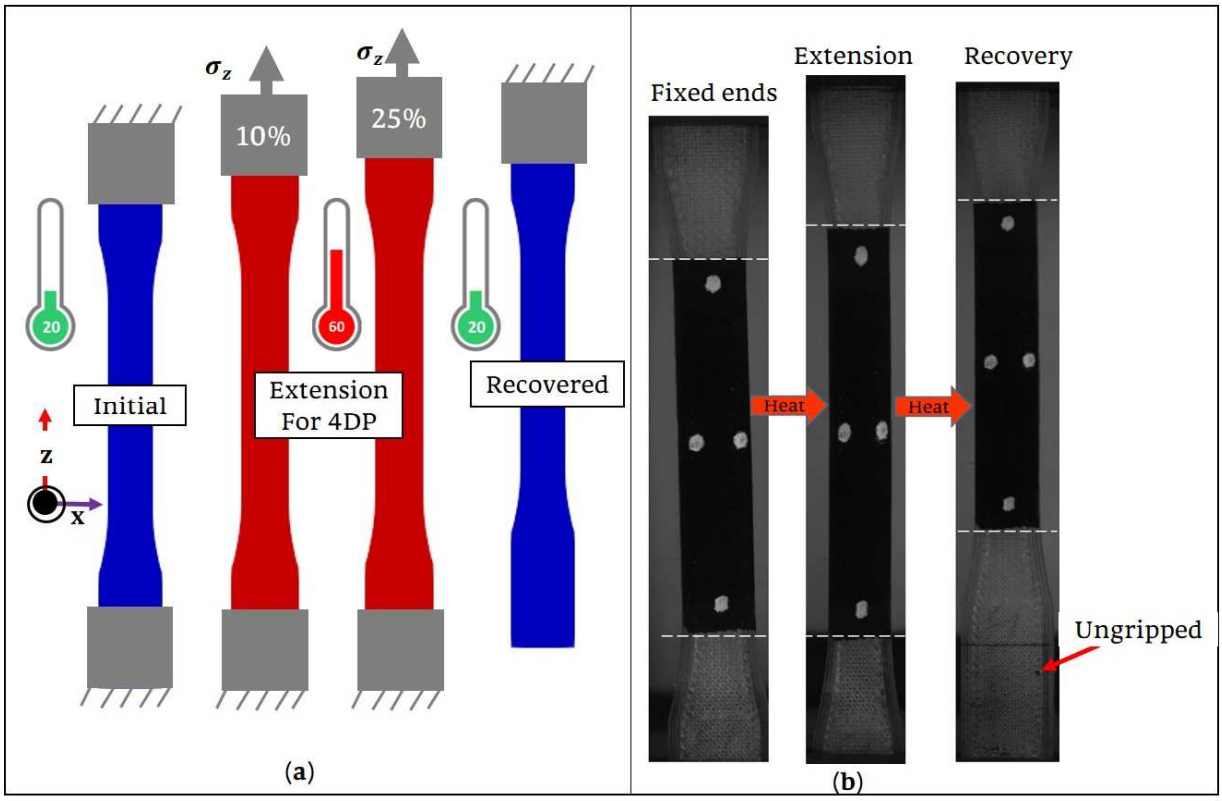

Fig. 6. Thermomechanical cycle setup for shape programming/recovery (a) Representation of thermal and mechanical conditions (b) Presentation of physically performed thermomechanical stages

3. Results and analysis

3.1 Investigation on SMP's behavior

4D printing of self-morphing structures is an exciting research domain with existing challenges however, it's hard to understand the shape memorability of SMMs without knowing the crucial thermomechanical properties of 3D printed specimens. Thereby the fundamental properties responsible for shape-programming and recovery are analyzed and discussed. In addition, the results of thermomechanical testing for shape programming/recovery of both processes were normalized to the same scale. Finally, the 10 % and 25 % normalized extension results of injection-molded SMP samples reported by Volk et al. [29] were compared with 3D printed at zero stress recovery in this study.

3.1.1 DSC analyses

Fig. 7 displays the DSC results of SMPC material, where the first normalized peak was prone to T_g, ranging from 44 → 48 °C in three succeeding tests, which is not far from the 45 °C provided by the manufacturer. The second subsequent plateau determines the degree of crystallinity at crystallization temperature starting from 89 to 99.4 °C to ensure the material is semi-crystalline. The third normalized peak populated the melting temperature span, which is almost similar at all heating rates. Importantly, a significant difference of nearly 10 °C in crystallization temperature

was noticed while selecting a heating rate of 1 °C.min^{-1}. Variable heating/cooling rates did not affect the glass transition temperatures but affected the crystallization temperatures and the degree of crystallinity. Meanwhile, how the degree of crystallization affects the shape memory properties is not yet addressed by the researcher's community.

Furthermore, Fig. 8 presents the DSC measurements of the SMPJ polymer, where only negative normalized peaks were observed in all three iterative analyses with no crystallization or melting peaks. This confirmed the material is a class of fully amorphous type SMP and holds a glass transition temperature between 47 to 50 °C. For SMPJ, the smaller heating/cooling rates (i.e., 1 °C.min^{-1}) lowered the glass transition temperatures to 2-3 °C. This means lower and higher heating rates could impact the activation of molecules chain mobility to enable shape recovery, these findings can be seen in the following sections. The curves present in Fig. 8 are very similar to other amorphous-type polymers analyzed by DSC elsewhere [14,32]. In addition, the T_g measures of SMPJ by current DSC experiments, by manufacturer, and from a reference study on the same material by DSC and dynamic mechanical analyzer (DMA) are classified in Table 4. The results obtained from DSC are very close to each other and quite far by up to 8 °C from the manufacturer value at a heating rate of 1 °C.min^{-1}, although the DMA values are almost the same as the manufacturer ones. However, the T_g value can be triggered to an upper limit while performing the physical aging on the printed samples and varying the heating/cooling rates [14]. Overall, glass transition temperatures obtained by the tanδ peak were higher than the ones obtained by DSC. This is very common; since T_g in DSC is taken at one-half of the increase in heat capacity, while T_g taken at the tanδ peak occurs after the shear loss modulus has peaked, thus reporting a higher T_g [32]. Finally, a higher T_g of SMPJ polymer than SMPC represents the presence of long molecular chains that can increase the polymer's chain mobility on activation to enable better shape memory properties.

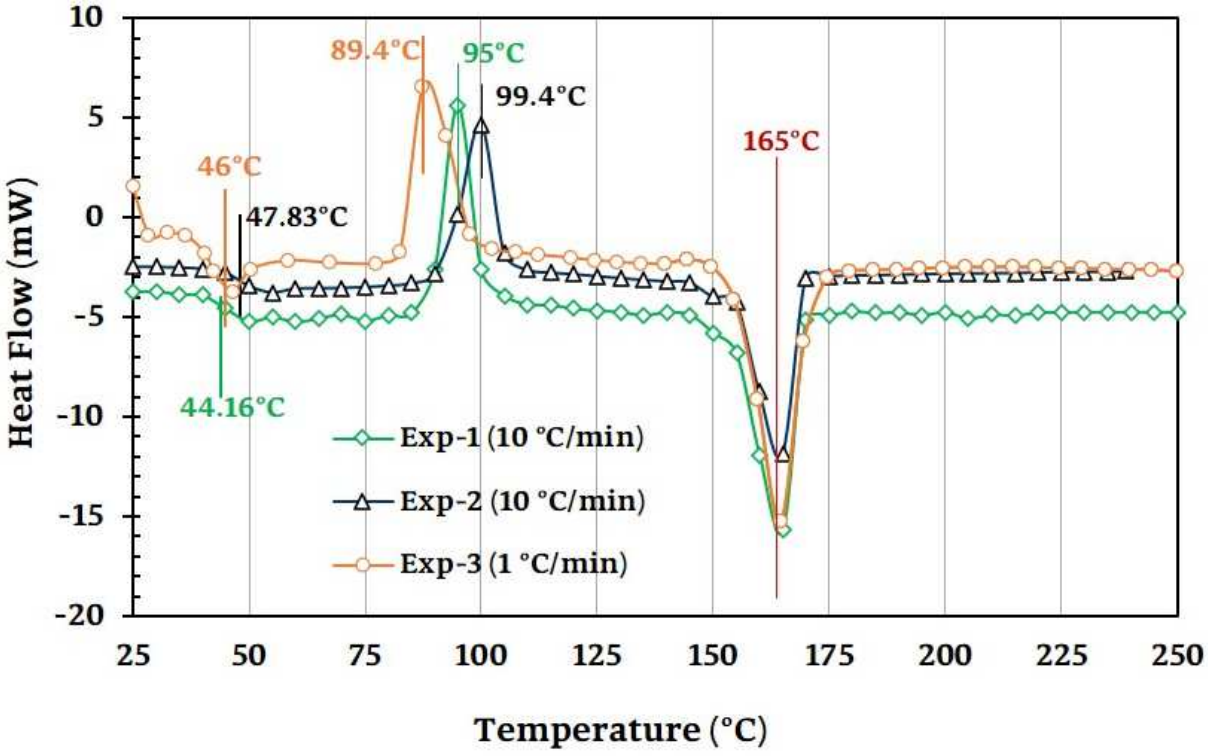

Fig. 7. DSC thermograms of semi-crystalline type SMPC for T_g evaluation at 1 and 10 °C.min^{-1}

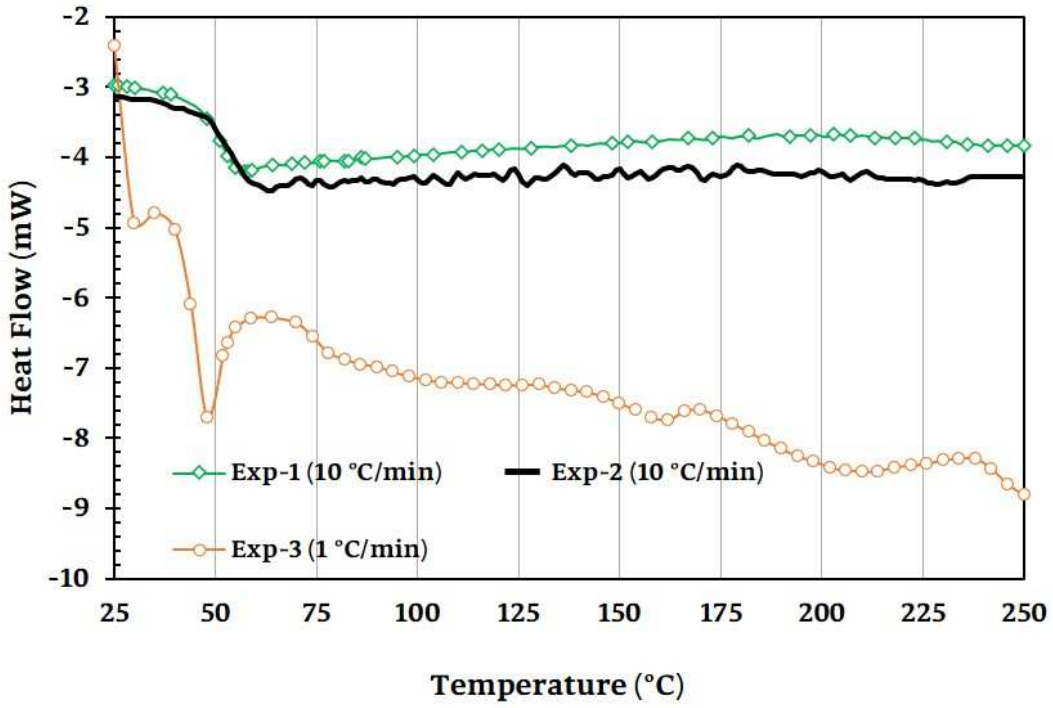

Fig. 8. DSC evaluation of amorphous type SMPJ for T_g at 1 and 10 °C.min^{-1}.

Table 4. Investigation of glass transition temperature following two different techniques

		Ref. T_g (°C)	T_g (°C) this Study	T_g (°C) by [32]	
Material	Exp. No.	Manufacturer	DSC	DSC	DMA
SMPJ	1	55	49.08	51.4	54.9
	2	55	50.12	52.0	N/A
	3	55	47.01	N/A	N/A

Specific heat capacity (Cp) as a function of temperature for both SMPs is shown in Fig. 9. Since thermo-responsive SMPs are very sensitive to thermal effects thereby, the study of temperature-dependent C_p could help to investigate the fundamental features of the phase transformation i.e., to determine the first-order transition in case of semi-crystalline type SMP characterized in this study. The highlighted blue and red points in Fig. 9. are the integral of C_p/T, also now as entropy (ΔS_{tg}) has reassured the T_g and C_p values of SMPC are around 48 °C and 1.498 $J.g^{-1}.K^{-1}$, respectively. Meanwhile, the T_g and C_p values of SMPJ are noticed at around 52 °C and 1.428 $J.g^{-1}.K^{-1}$. The excessive heat capacity during the modulation has good agreement with the C_p diagram of SMPJ type polymer reported by G. Baer. [32] through a similar DSC approach as reported here.

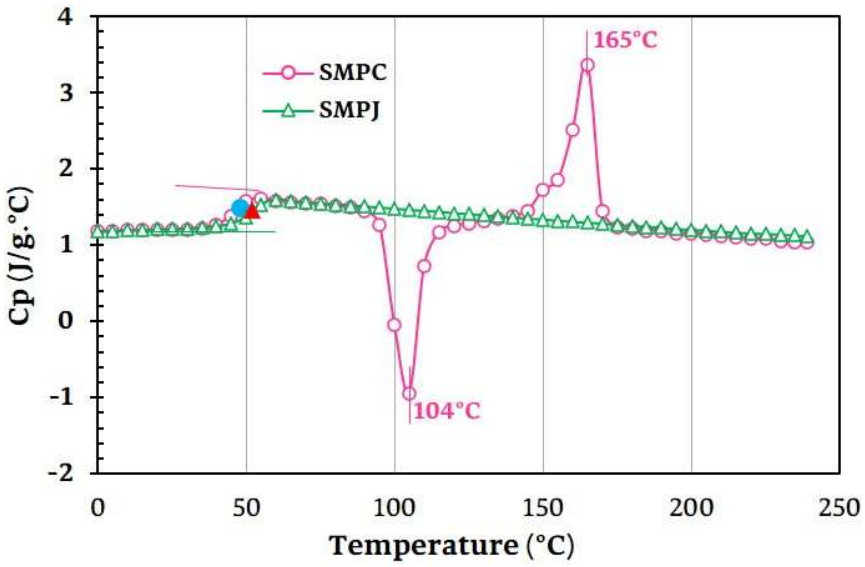

Fig. 9. DSC measurements curves of SMPC and SMPJ for temperature-dependent C_p values

3.1.2 Thermogravimetric analysis (TGA)

In the case of variable printing and shape programming temperatures, the thermal decomposition kinetics or percentage weight loss of molecules of both SMPs are crucial for understanding storage modulus, strain energy, and shape fixity behavior [38]. Accordingly, the thermal stability analyses were performed using a thermogravimetric analyzer (TGA/DSC 3+)

surrounding the nitrogen purge (20 mg.min^{-1}) to determine the safe use of printing and programming temperatures. TGA/DSC 3+ by Mettler TOLEDO facilitates the simultaneous examination of weight reduction and heat flow above melting temperature [39]. The experiments were conducted at a heating rate of 5 °C.min^{-1} and 10 °C.min^{-1} between 25 to 600 °C.

Fig. 10a illustrates the percentage weight loss and heat flow (HF), where the heat flow sensor precisely measured the melting and crystallization events in the function of temperature change. Overall, both SMPs at variable heating rates showed significant decomposition and heat flow following a temperature range of 300–400 °C. In this range, the weight loss of SMPJ at 5 and 10 °C.min^{-1} was reduced to 69.5% and 47.6% respectively. Whereas almost 100% sudden degradation of SMPC has occurred at 10 °C.min^{-1} between 300–400 °C, which is significantly higher than SMPJ polymer. A detailed description of the weight loss history at 5 °C.min^{-1} is presented in Fig. 10b, where the SMPJ thermal degradation or decomposition started at an initial temperature of 305 °C, which decreased gradually to reach the highest thermal decomposition at around 343 °C and ended nearly at 400 °C. Eq. (1) presented the weight loss factors to normalize the thermal decomposition data points [33]. Whereas w_i is the initial weight of the specimen before TGA, w_f denotes the final weight after TGA loss, and w(T) indicates the weight at temperature T.

$$\text{Reduced weight (\%)} = \frac{w(T)-w_i}{w_i - w_f} \quad (1)$$

The thermogravimetric analysis measured the change in polymer molecular weight loss as a function of temperature which helps to predict the thermal stability and material flame retardancy range [40]. Ultimately, the thermal stability of amorphous type SMPJ polymer is seen way better than SMPC polymer. The overall TGA thermal decomposition tendency is very similar to one that has been analyzed by Zhao et al. [38] on PLA/ Fe_3O_4 composite material.

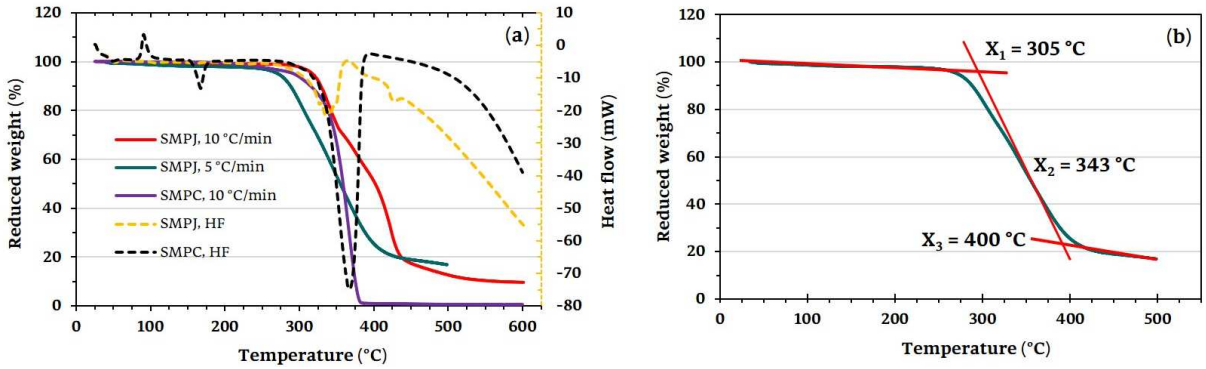

Fig. 10. Curves of thermogravimetric analysis (a) Weight loss and heat flow analysis of SMPC and SMPJ polymers(b) Description of weight loss of SMPJ at 5 °C.min^{-1}.

3.2 Thermomechanical shape memory signatures

3.2.1 SMS mechanics during heating

The experimental time-temperature graph illustrated in Fig.5 denotes a complete thermomechanical cycle at a temperature rate of 3 °C.min^{-1}. The specimens produced by injection molding were tested at 3 °C.min^{-1}, however, an end recovery temperature was set to 90 °C, mean

T_g + 25 °C [29]. However, the 3D-printed SMPJ specimen didn't endure even around 80 °C for a longer holding time without physical aging and exhibited limited thermomechanical durability and higher thermal strain [11]. Therefore, a T_g + 10 °C (i.e., 60 °C) was noticed as a better shape programming temperature where the material is supposed to reach 100% into the rubbery state to perform full phase transformation. A gradual increase in temperature inside a precisely controlled environmental chamber transferred the glassy (hard and brittle) phase into the rubbery (soft and viscous) phase progressively. After initial heating to cross the passive (glassy) state of the polymer, a T_g above temperature was kept constant to apply extension or deformation for shape programming. A higher heating rate of 10 °C.min^{-1} for the shape recovery cycle can delay the stress-free strain recovery and in some cases increase the amount of irrecoverable (residual) strains [37], therefore, all SMS heating cycles were designed to a maximum of 5 °C.min^{-1}. In addition to temperature rates, the thermomechanical experiments in tension mode were performed at 2 mm.min^{-1} of loading rate, similar to the loading rates of 1- 50 mm.min^{-1} recommended for semirigid ASTM D638-type polymeric structures [27].

3.2.2 SMS mechanics during cooling

To investigate the SMSs properties of 3D printed SMP specimens, the deformed temporary configuration of the object should be fixed upon cooling below T_g [9]. Like the heating cycle, the cooling cycle (Fig. 5) is programmed at 3 °C.min^{-1} to drive the temperature below T_g and fix the temporary shape in the brittle or hard phase. For multiple SMS transitions, a persistent heating-cooling cycle is recommended. A higher cooling rate of 10 °C.min^{-1} might not introduce a significant impact on shape memory behavior however, a tenfold longer cycle time will be prominent in the case of performing a thermomechanical cycle at 1 °C.min^{-1} than at 10 °C.min^{-1} [29]. Meanwhile, with the application of lower cooling rates, the stress relaxation might need a smaller pace to reach the required thermal stability. In this context, Lei et al. [41] proposed that stress relaxation is dependent on the state of the temperature, and structural relaxation itself. In contrast, at a higher cooling rate, the time needed to reach thermal stability can exceed several minutes. During cooling, the pre-loading used for shape programming and other boundary conditions should stay constant. Once the temperature reaches room temperature (Tr), the polymer will be in a purely elastic region of the glassy state, and the total freezing stress in the cooling range (70 to 20 °C) to keep the fixed shape without external load at this state can be calculated through Eq.(2) [36].

$$\sigma_{fr}^{total} = \sigma_{max} - \sigma_{min} \quad (2)$$

Where $\sigma_{\mathrm{fr}}^{\mathrm{total}}$ represents the total freezing stress increased during the cooling stage, σ_{max} denotes the maximum stress response after cooling, and σ_{min} determines the minimum stress noticed during the cooling process. The cooling stress evolutions are presented in Fig. 14. The main influencing factors leading to stress evolution during the cooling process are; stress relaxation time, induced thermal stress level, and increased or decreased elastic modulus, respectively.

3.2.3 Uniaxial stress-extension relationships

To realize and compare the 3D printed and injection molded parts behavior at different temperatures, the quasi-static uniaxial tensile tests were performed at a dual column desktop type INSTRON® of 50KN capacity as presented in Fig. 3. The standard practices were adopted

explicitly according to ASTM [27] "for small extensions of < 20% the extensometer strain error should not exceed 0.001 and in case of high extension experiments the measuring instrument shall be less than ±10%". Fig. 11 illustrates the results of uniaxial tensile tests performed at room temperature (20 °C) and above T_g at 60 °C for a fixed 5 % of extension to see the temperature affecting the mechanical properties. The stress-extension results are linear in case of extension above T_g temperature, and the material exhibit super-elastic behavior without presenting any fracture however, the tensile stress is limited to 0.15 MPa. Although, the stress extension at room temperature did not reach 5% of applied strain and instead fractured at 3 % due to glassy entanglement and limited molecular chains mobility with a maximum yield stress of 35 MPa, which is 234 times higher than the one measured above T_g.

Here the elastic to plastic range threshold for tensile stress at room temperature did not cross the 2 % of strain (ε), although this applied strain % could reach above 100 % in case of extension above T_g which afterward could be released on applied thermal stimuli [42]. Aberoumand et al. [14] proposed the physical aging of the FFF printed sample to improve their mechanical and thermal properties. They used PET-G filament to produce prototypes with a FFF printer and performed aging between 48-120 h at 55 °C and reported a 10-15 % increase in the yield stress, and homogenized the thermal strain to have minimal shrinkage. Although the SMPJ used in this study can't withstand the dimensional performance to perform physical aging, the structure reported a drastic strain-softening and self-contraction at a higher temperature holding for a long time.

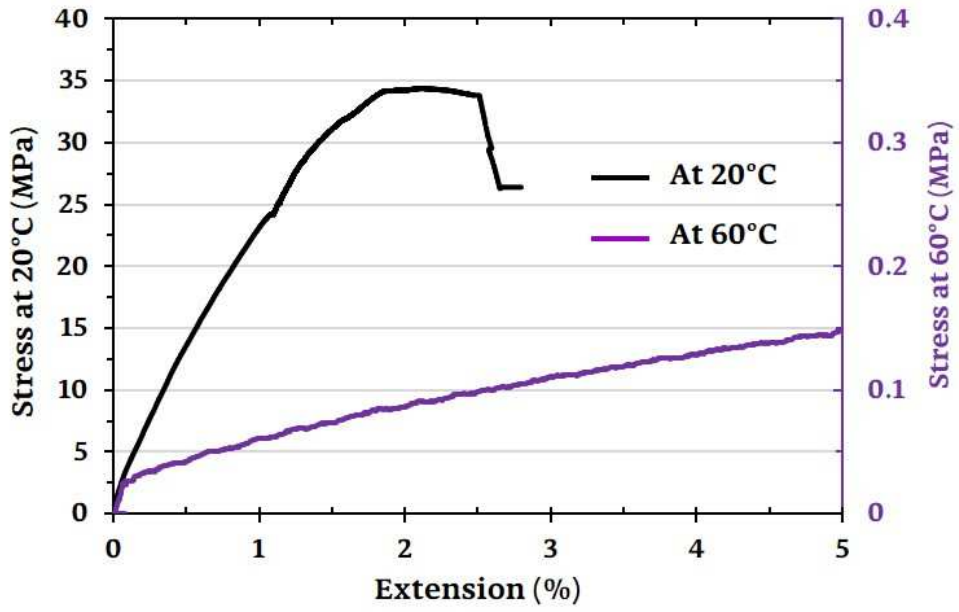

Fig. 11. Experimental stress-extension relationships of SMPJ at glassy and rubbery states at fixed 5% of extension.

3.2.4 Influence of heating rates and peak strains

Fig. 12 plots and correlated the recovered extension versus reheating temperature and percentage shape recovery ratios versus recovery temperature of 3D printed and injection molded specimens. Results depicted in Fig. 12a presents the stress-free shape recovery behavior of 25 % extended specimens at different heating rates for shape recovery although, all the heating and cooling rates were fixed and identical for 3D printed and IM-produced samples such as 1, 3, and 5 °C.min^{-1}. SMPs shape memory could be triggered, through stress-free strain recovery, fixed-strain stress recovery, or constrained displacement recovery [28,43], whereas most studies discussed stress-free strain recovery [4,9,11,22]. Accordingly, to capture the stress-free recovery in a continuous environment the AVE-2 extensometer worked as a digital image correlation (DIC) instrument (Fig. 3). Similarly, while maintaining identical constraints to IM test/results such as thermal stability time, loading/unloading speed, etc. the investigation of varying temperature rates not only enabled the reduction in the potential cycling time, but it indicates the significant differences in recovery ratios that kept increasing to recover even on the constant temperature of 70 °C during the thermal stability period (Fig. 12b). However, the difference in percentage recovery is due to accumulated strain storage and residual induced stresses generated during shape programming at different rates.

Both 3DP and IM-produced specimens started to release the stored strain for stress-free recovery before even reached to T_g. Especially, Fig. 12b demonstrated that the specimen tends to a recovery temperature of 1 °C.min^{-1} started to recover earlier around 42.6 °C then recovery begins around 46.62 °C in case of heating at 5 °C.min^{-1}. This proves that the stress-free recovery behavior is not only influenced by induced strains and stresses during the programming step as reported by [16,22], although, the heating rate also has a significant impact. The shape recovery relation with temperature increase above T_g is linear/smooth during all heating rates for 3DP samples, however, a sharp shape recovery behavior is noticed in the case of IM-produced samples once they crossed the glass transition temperature. These phenomena reflect that 3D printed structures became weaker or more elastic above T_g than IM produced. Similar to sharp recovery at higher temperatures, Ly and Kim, [15] performed the structure's programming/recovery experiments at different temperatures and reported a significant influence on recovery time while recovered at a higher-end recovery temperature. They mentioned it took 7 seconds to recover at a temperature higher than T_g, than recovery performed exactly at T_g temperature which took 42 seconds. A 100% shape fixity ratio was measured in all the series of tests, therefore, only the shape recovery ratio (a crucial part of thermomechanical shape memory testing) is discussed in this work. The shape recovery percentage for 3D to 4D printing of temporary shapes is measured as follows: where $3DP_{ori}$ is the original dimension of the 3D printed sample, 4DP present the dimensions of the temporarily programmed form for 4D printing, and $3DP_{rec}$ is the recovered form from 4DP towards initial dimensions.

$$R_r = \frac{3DP_{rec \rightarrow 4DP}}{3DP_{ori \rightarrow 4DP}} \times 100\% = \frac{3DP_{rec-4DP}}{3DP_{ori-4DP}} \times 100\% \quad (3)$$

There are several reasons for the linear recovery of 3DP samples, i.e., the different heating rates might be controlled more precisely to enable the polymer chains to release the stored strain gradually while reheating until T_g+20 °C. On contrary, the environmental chamber used to

program/recover the IM samples might not be controlled with similar precision. In addition, the higher-end recovery heating until T_g+25 °C than general cases of T_g + (10→20) °C, and finally, the homogeneous induced strains are all factors to have the sharp shape recovery curves [35]. Overall, the maximum shape recovery of 95 % is seen in the IM specimen at a heating rate of 1 °C.min^{-1}, following the 93% of the 3D printed part at a temperature rate of 2 °C.min^{-1}. Furthermore, the 3DP specimen's shape recovery kept raising at the end of the recovery temperature (70 °C), this is due to shape relaxation at a constant temperature, meanwhile, this constant temperature time was kept like the time needed to reach 90 °C end recovery temperature for IM samples. This phenomenon is attached to the structural relaxation and a viscoelastic/viscoplastic property of SMP which kept growing gradually, as reported by Lei et al. [41]. A higher end-recovery temperature can increase the molecular chain mobility to enable a better and faster shape recovery percentage [15]. The variable reheating rates and geometric homogeneity of IM-produced specimens weightily affected the shape recovery ratios as seen in Fig. 12.

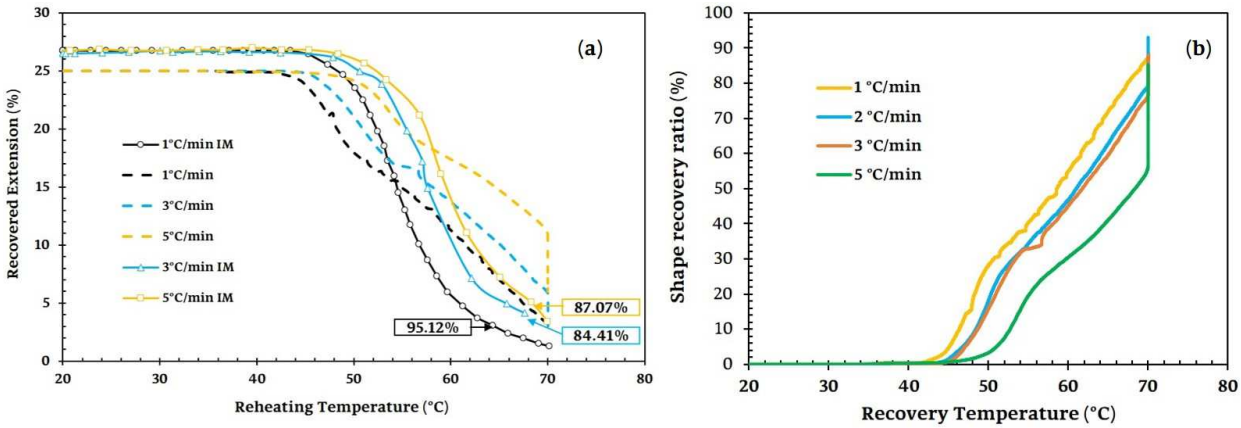

Fig. 12. Shape recovery behavior analysis at different heating rates (a) Comparison of 3DP and IM specimens recovered at 1, 3, 5 °C.min^{-1} (b) Analysis of shape recovery ratios of 3DP samples at 1,2, 3, and 5 °C.min^{-1}

Fig. 13 enlightens the recovery times at varying heating rates for a fixed end-recovery temperature of 70 °C. The recovery time is broadly dependent on the reheating rate of shape recovery. At a reheating rate of 1 °C.min^{-1}, initially, the temperature profile is quite non-linear, especially, during a temperature rise between 30 → 36 °C which took more than 13 minutes to just cross a temperature range of 5-6 °C. Despite that, the time-temperature relationship is quite linear while heating at a rate of 5 °C.min^{-1}. In addition, from this recovery part of the thermomechanical cycle, it can also be noticed that the recovery time is fourfold while heating at 1 °C.min^{-1} than 5 °C min^{-1} which is quite long, challenging, and expensive for engineering applications. Therefore, depending on the application, external/internal environment a specific heating rate with an appropriate time to fully activate the shape memory properties is needed to standardize the thermomechanical programming efforts for a given material and application.

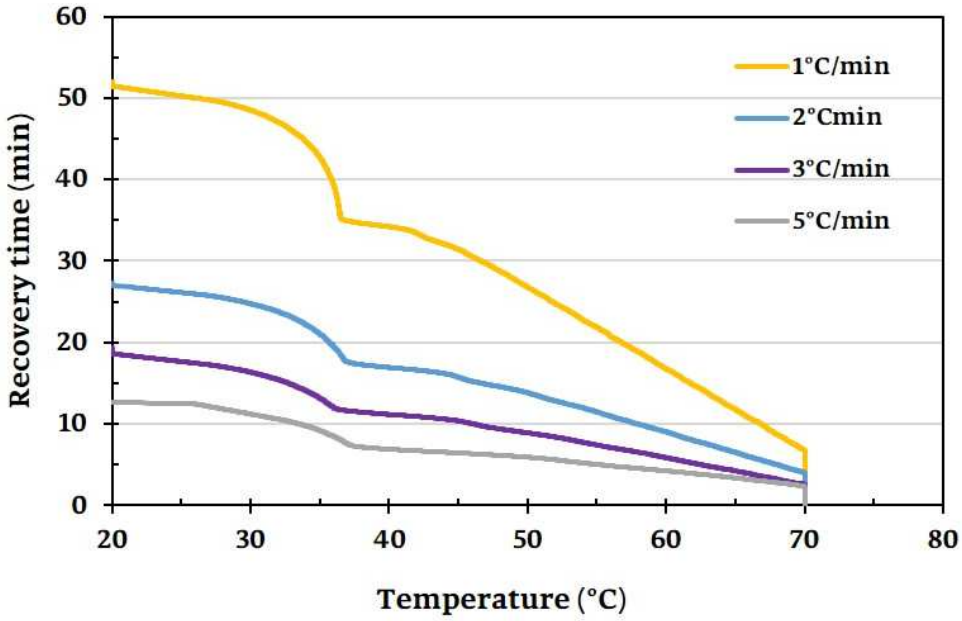

Fig. 13. Effects of heating rates on recovery time

The multiple states of the thermomechanical cycle for shape memory effects analysis are already described in Fig. 5, which are the means to shape programming at a constant temperature and recovery at varying temperatures. Whilst the shape recovery to reach the initial reference configuration from the actual configuration is prone to perform at precisely controlled rising temperature rates starting from room temperature until above glass transition temperature in the case of polymers. However, the activation of the polymer chain mobility (responsible for stress-free recovery) does not correspond only to sudden temperature change but rather involves time to equilibrium state [41]. In addition, the shape recovery performance was noticed to be dependent on the induced pre-strain stored during the programming cycle. Xiao [34] plotted the recovered strain with temperature from numerical and experimental results and highlighted the shape recovery performance of ABS resulting from the release of pre-strain storage during shape programming. Accordingly, Fig. 14 shows the percentage of recovered extension/strain versus time to the deformed configuration during shape programming. Since the release of induced thermal strain in polymers is time-dependent, therefore, the thermomechanical programming/recovery time is a key factor to perform a complete cycle in minimum time for engineering applications of self-assembling structures and controlling the major operational costs (i.e., equipment, labor). The thermal stability time of up to 25 minutes defined by Volk et al. [29] in the case of IM specimens is eventually very long. The effort to reduce such a longer thermomechanical cycling time is therefore considered in this present study. On this matter, Fig. 14 showed how temperature rates affected the recovery % and how long the dwell time could be, which is clearly illustrated.

As seen at a reheating rate of 1 °C.min^{-1} for recovery, the specimen recovered up to 90% in the first 28 minutes, and then with the increase of almost 45% dwell time no further change in

recovery ratio has been seen. Alongside, while selecting a reheating rate of 5 °C.min^{-1} for recovery, the total shape recovery is reported in the defined recovery cycle time with a least or negligible dwell time. Finally, reheating at 2 and 3 °C.min^{-1} for recovery spotted a normal dwell time with better and similar recovery ratios. Therefore, a 1 °C.min^{-1} heating/cooling rate is not recommended for multiple applications due to the very long cycle time and slower shape memory recoveries. Furthermore, to minimize the recovery time rather than varying the heating rate, the final recovery temperature above T_g could have significant effects as reported elsewhere [15].

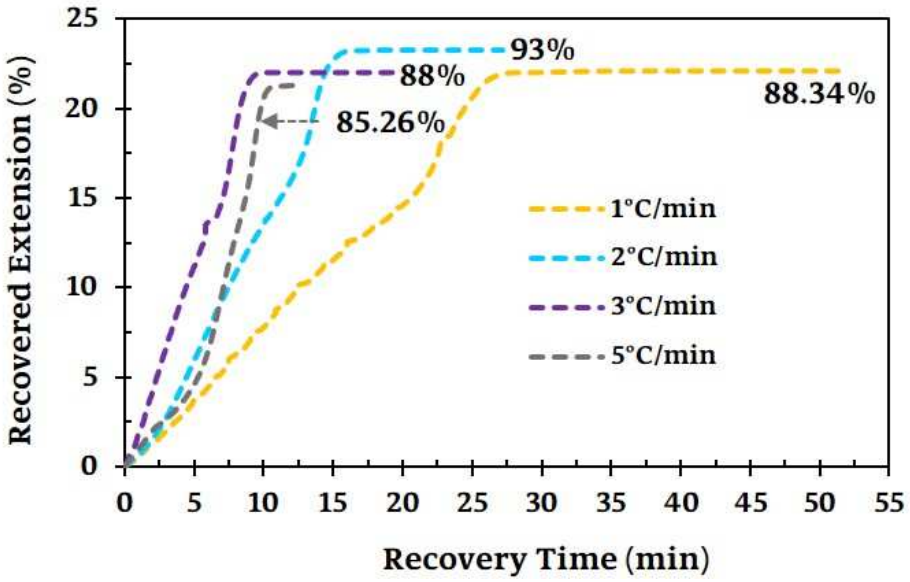

Fig. 14. Analysis of recovery percentage about 25% extension depending on heating rate starting from 1-5 °C.min^{-1} for 3D printed specimens

Fig. 15 shows the percentage of shrinkage strain measured along the transverse direction (ε_{xy}) of the ASTM D638 dog bone samples. The shrinkage percentage was measured using an AVE-2 extensometer using the reference configuration of the transversely defined dots in Fig. 4. The objective was to analyze the percentage recovery of shrinkage strain during the loading cycle in ε_{xy} direction of the longitudinally extended specimens at variable heating rates. All the results equated in Fig. 15 are for 25% extension at 1, 2, 3, and 5 °C.min^{-1} temperature rate. The percentage shrinkage during loading to 25% extension is measured and plotted in Fig. 15. Similarly, the recovered percent shrinkage strain of the transverse direction is due to heat exposure at varying heating rates as compared to the initial shrinkage value during the loading cycle. At a heating rate of 1 and 2 °C.min^{-1}, the specimen recovered to 111.72% and 102.81% receptively.

The recovery percentage beyond 100% is belonging to the thermal contraction (thermal strain) of 11.72% and 2.81% due to the longer constant heating delay (dwell time discussed before) introduced at slower heating rates during the thermomechanical cycle. Although, a heating rate of 3 °C.min^{-1} presented 100% shape recovery without extra thermal contraction following a transverse direction ε_{xy}. Consequently, a heating rate of 5 °C.min^{-1} showed less than 100% recovery from one measured during the loading cycle. The higher cooling rate such as 5 °C.min^{-1}

provided less time for the rearrangement of the polymer networks limiting the 100% recovery of the transverse deformation [41]. Meanwhile, increasing the heating rate from 1→5 °C.min^{-1} denotes a decrease in transverse shape recovery.

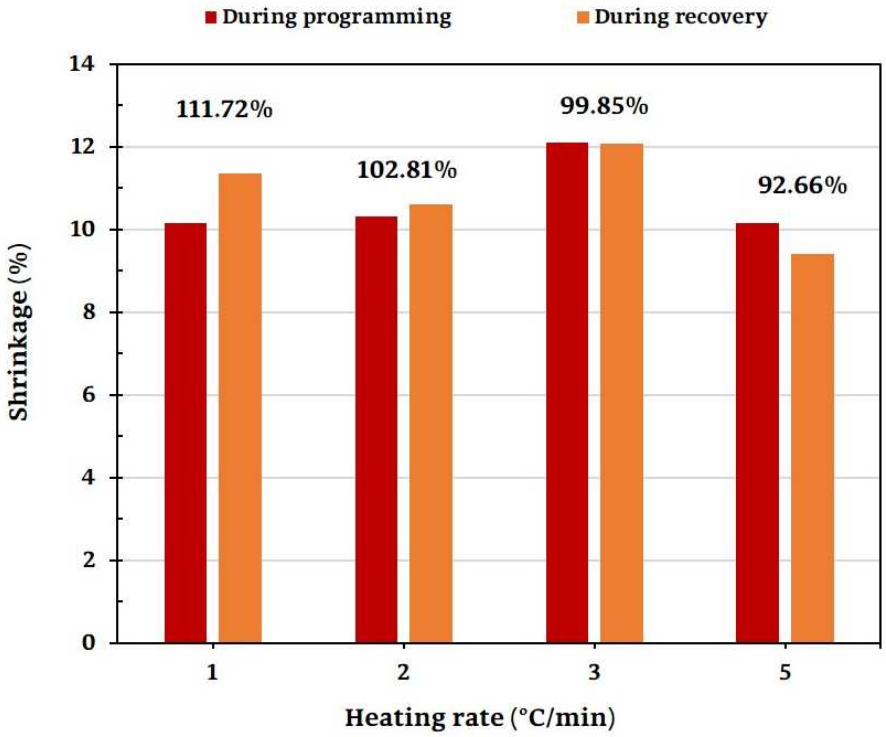

Fig. 15. Analysis of temperature rate-dependent recovery of the transverse deformation

Here Fig. 16, portrays the shape recovery behavior of IM and 3DP samples tested at 10 % and 25 % peak strains. The extension recovery trend of IM and 3DP specimens are likely in the event of a 10 % peak strain. However, the stress-free strain of the 25 % extended IM sample showed a quick release to recover in a smaller fraction of time as compared to 3DP. In both cases, the AM-produced samples recovered better in a linear transition mode than IM-produced parts, especially for 25 % peak strain. In addition, the 25 % extended specimens recovered faster between 45 °C and 60 °C than the 10 % extension, this is due to the level of pre-stored strain, usually higher due to high induced strain of 25 % than 10% [19].

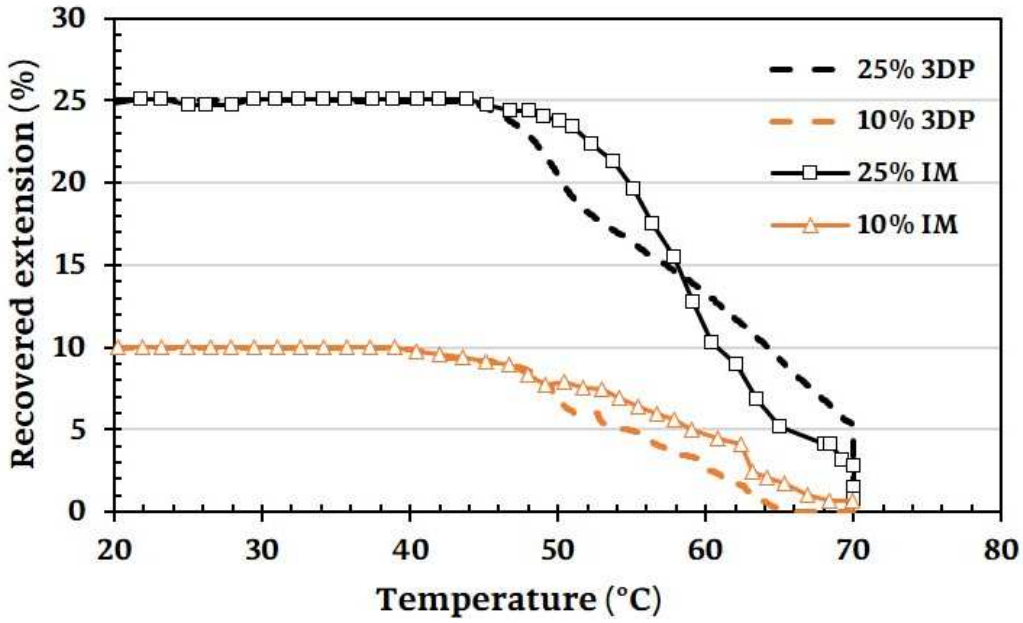

Fig. 16. 3DP and IM recovered extension-temperature relationship at 2 °C.min^{-1} for 10% and 25% of extension.

3.2.5 Stress behavior of recovered specimens

Fig. 17 depicts the heating-cooling cycle, where during the cooling process below T_g the object's stress gets recovered due to the frozen state of molecular chains that allow fixing the programmed shape. Meanwhile, to distinguish the effects of fabrication process variability on recovered stress during the cooling phase, the SMS cycle for shape programming was fixed for a maximum strain value of 25 %. In addition to process variability, the heating/cooling rates of both IM and 3D printed specimens were programmed and recovered at 1 and 5 °C.min^{-1}. Fig. 17a outlined the recovered frozen stress during the cooling cycle at 1 °C min^{-1} of IM produced and 3DP sample which increased drastically as soon the temperature decreased from 40 → 30 °C. Although, the 3DP specimen's frozen stress increased gradually and reached up to 0.8 MPa as compared to twofold (1.6 MPa) in IM recovered sample. This difference might be due to incomplete transition and limited heterogeneous pre-strain storage in the weakly bonded layers of the 3D printed parts and homogenous strain distribution in the case of the IM process [29]. Similar to the results presented here, the FFF printed and programmed rectangular specimens by Aberoumand et al. [14] indicated recovered frozen stresses of 1.24 and 0.92 MPa with distinct printing parameters. Meanwhile, the recovered stress at 5 °C.min^{-1} (Fig. 17b) is limited to 1.2 MPa of IM and three times less in the case of a 3D printed sample. This is the fact of rapid heating/cooling which enabled rapid release/lock of induced stresses to certain temperature values [35].

From the extension-recovery cycle point of view, the shape programming cycle followed similar variations for both cases with agreeable time distributions. However, the extension of 3DP samples exactly controlled around 25% while using the experimental setup discussed before (Fig.

3). Furthermore, at 1 °C.min^{-1} thermomechanical cycle, the shape recovery of the IM specimen took 37.5% less time and 8% better recovery than the 3DP sample. This is due to the end recovery temperature of the IM part being maximum temperature (T_g+25 °C) enabled the quick release of stored strain as compared to lower-end temperature recovery (T_g+20 °C) on the 3DP sample. The current issues of dimensional stability of the 3DP part to perform quick shape recovery at higher-end temperatures might be optimized with the physical aging process proposed elsewhere [14,34]. It's important to remember that sometimes programming at higher temperatures and loading performed very slowly can lock the structure into a permanently deformed shape that can't recover at all, [34].

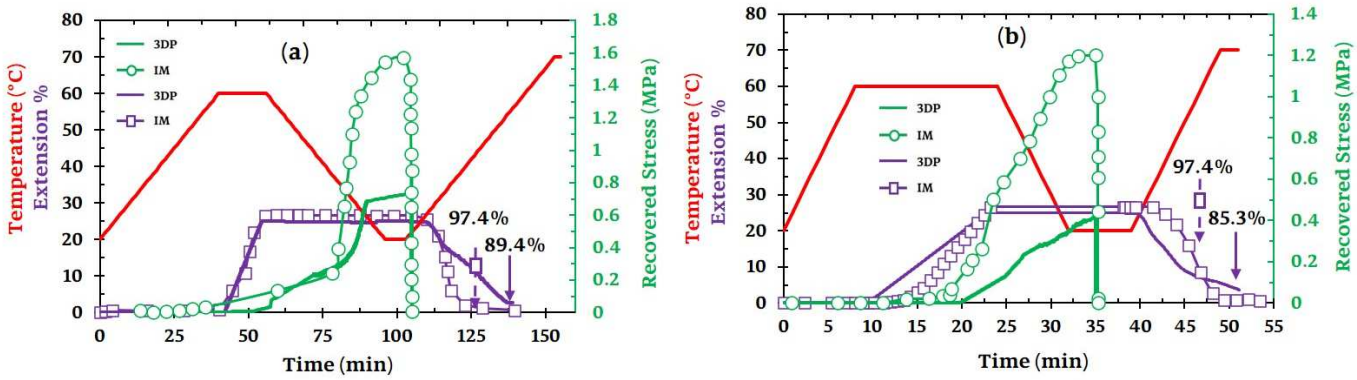

Fig. 17. Recovered stress-extension behavior of 3DP and IM samples (a) At 1 °C.min^{-1} and 25% nominal extension (b) at 5 °C.min^{-1} and 25% least extension

The hot and cold programming stresses at above T_g and room temperature for 5% of extension are already demonstrated in Fig. 11. Usually, the thermal effects have a significant influence on the mechanical properties therefore, how the shape programming/loading stresses for up to 25% of the extension will evolve, linearly or non-linearly is depicted in Fig. 18. Since SMPs shape programming needs to perform above T_g which mainly requires limited stress. In this context, Kallel et al. [16] reported loading stress of 0.3 MPa while programming the specimens at 60 °C. In addition, Fig. 18 shows the loading/programming stress of IM and 3DP structure of a similar nature and extended for similar extensions. In both cases, higher loading stress is reported at higher heating rates. Injection-molded specimens resist limited programming stress due to the length of up to 25 minutes of thermal equilibrium time above T_g, which regularizes the chain entanglements and limit the internal stresses reported before shape programming.

In contrast, to speed up the thermomechanical testing for multiple cycles, the thermal stability time to recover elastic deformation was kept constant for 120s in all shape memory tests performed in this study. The lower thermal stability and higher heating rate limit the programming stress to 0.33 MPa, but the cycle time is reduced up to tenfold compared to the cycles defined for IM samples. Since stresses are released from the polymer as the temperature gets stable with time increase, therefore, a longer temperature-dependent relaxation time can improve the shape recovery ratio up to a few chunks. In contrast, as time passes the shape fixity ratio can decrease because of the molecular chain's mobility causing structural relaxation and slipping from the fixed configuration after the unloading position. The stress relaxation effects mainly affect the shape

recovery and fixity ratios if the temperature is near to glass transition region [41]. Similarly, the shape fixity time could be minimum during unloading around low temperatures as compared to high temperatures.

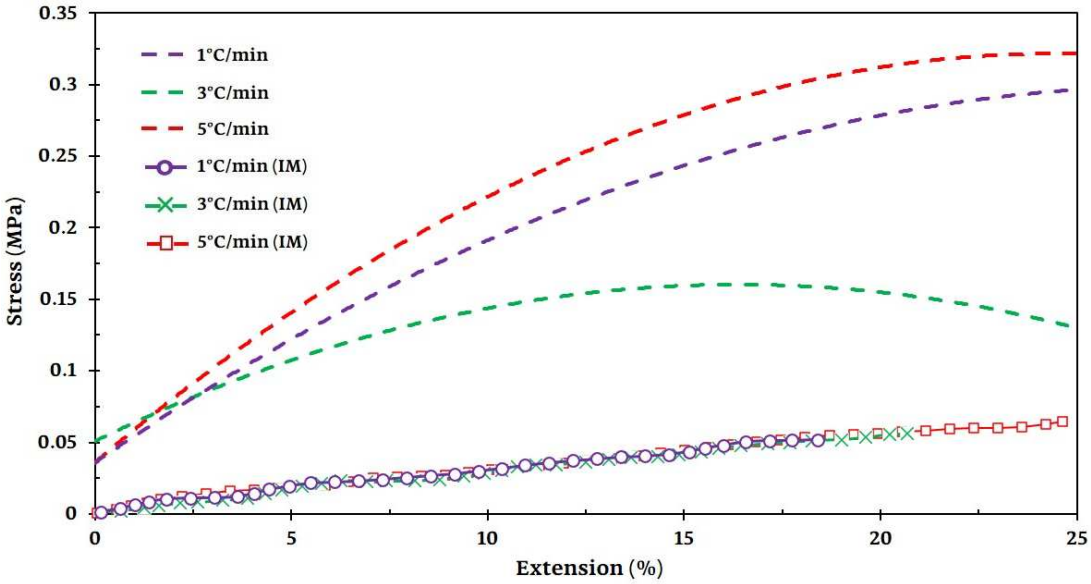

Fig. 18. Comparison of 3DP and IM stress-extension relationship at 1, 3 and 5 °C.min^{-1}

3.2.6 Macro morphological analysis

The macro or microstructural assessment of the recovered specimen after shape programming can provide additional insights into the cell entanglement or realignment after following shape extension, fixity, and recovery behavior in counterpart to the as-printed specimen. Instead of 3D printing, Zhao et al. [44] manufactured a smart releasing cylindrical device with shape memory polymer composites using a conventional molding technique. They performed the SEM analysis before and after the strain release for shape recovery and did not see any macro morphological damages, however, slight micro-morphological damages were present in highly compressed specimens.

In this context, a scanning electron microscopy (SEM) analysis was performed on the FFF printed and recovered specimen that revealed the samples studied here have not seen specific fractures, instead of a few shrinkage and expansion effects due to thermomechanical loading. Therefore, in this study, the mid-printed infill cells fabricated at 90/0° raster orientation (presenting a square shape) were selected for an optical microscopic assessment, and the cell size of the as-printed specimen is measured to compare with the after-recovery specimen. Analyzing the infill square cells while crossing the three ± 45° top solid layers as possible at the expense of the optical image quality. Fig. 19 illustrates the cell sizes in the X and Y axis that were 3D printed and whose X, Y, and diagonal lengths were evaluated using optical microscopy at a magnification of 50x (500 µm). Cell size data collection is performed two times at two different positions around the unique selected section of each specimen.

Fig. 19a presents the cell sizes of as-printed specimens for reference configuration to compare with the recovered ones tested at different peak strains and heating rates.

Fig. 19b shows the specimen programmed for 25% extension and recovered at 1 °C.min^{-1} heating rate, which encompasses the similar openings of the cells in the XY axis in comparison to its initial configuration. Meanwhile, the extension-recovery tests slightly displaced the cells in the XY axis which enlarged their diagonal length from 1047 µm to 1077 µm respectively.

Fig. 19c presents the cell sizes of specimen extended and recovered to 25% at 2 °C.min^{-1}, which exhibited almost similar configuration to their initial as-printed object, which reaffirms the effects of maximum recovery ratio obtained at a heating rate of 2 °C.min^{-1} as seen in the previous section. Finally, the effects of different peak strains of 10% with a similar heating rate of 2 °C.min^{-1} can be seen in Fig. 19d.

Qualitatively, the XY cells for the 10% peak strain recovered specimen are perfectly straight and identical to the as-printed specimen, however, the cell's alignment of 25% extended specimens is lightly bent inside, especially the one parallel to Y-axis which increased their diagonal lengths collectively. Quantitatively, no special changes in cell reduction have been seen. Overall, the variations in cell sizes for identical specimen sections are due to the combined effects of the printing process [45] (i.e., discontinuities of filament extrusion, imbalance heating cooling effects, etc.), thermomechanical shape memory cycle [46] (i.e., the heating rate, holding time, end recovery temperature, etc.), and the cell location itself (i.e., near to the wall, in the center, etc.). Overall, a 25% shape programming and recovery of the dog bone gauge length under a higher temperature did not present interesting macro or microstructural changes, therefore, the SEM analyses of such structures potentially needed higher deformation (i.e., 50% to the gauge length) at heating level below T_g.

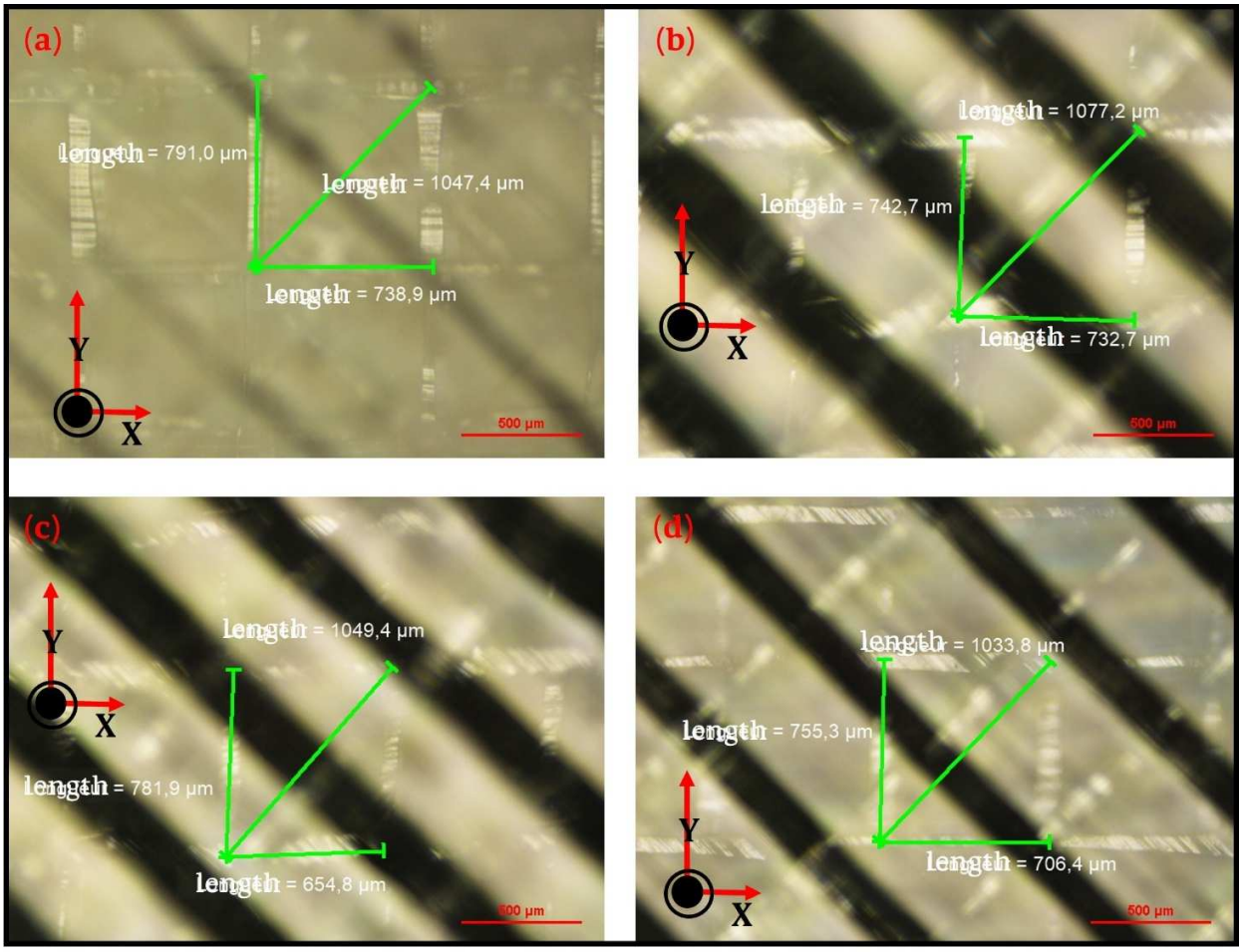

Fig. 19. Optical assessment of the center section of FFF printed specimen (a) Analysis of as-printed specimen (b) Analysis of 25 % extended and 1 °C.min^{-1} programmed/recovered specimen (c) Analysis of 25 % extended and 2 °C.min^{-1} programmed/recovered specimen (d) Analysis of 10 % extended and 2 °C.min^{-1} programmed/recovered specimen.

4. Conclusion and perspectives

Initially, thermal transitions of semi-crystalline and amorphous type polymers were investigated, including glass transition, crystallization, and melting temperatures. Further investigations, such as the change in specific heat capacity and material stability as per temperature variations were also examined during the analytical computations of this study. Those characteristics provided insights into the polymer's nature to withstand the thermomechanical loadings and precisely define the shape programming and recovery behaviors influenced by temperature change. The SMPs investigations are based-on thermomechanical shape memory signatures (SMSs) influenced by two different manufacturing processes, especially due to the formation of crystallization properties during the fabrication process and distribution of small to large pre-strain induced during shape programming cycles. The FFF-produced structures reported heterogeneous induced strains, higher in the bottom layers than in the top and programming steps, that directed a slower strain

release and structural relaxation during stress-free strain recovery and took longer times to enable a full recovery.

Although, the IM-produced specimens presented sharp strain release and 5-10% better shape recovery ratios above T_g due to their homogeneously distributed pre-induced stress/strains and higher end-recovery temperature. The lower heating rates results in a higher shape recovery percentage due to a long enough time for strain release and structural relaxation, although prone to very long cycle time that can also induce significant thermal shrinkages if the material is not introduced to the thermal treatments or physical aging process. A higher heating rate can enable agreeable shape recovery up to 90% in case the end recovery temperatures were clearly defined, along with appropriate thermal stability holding time that might need additional measures to achieve the required shape recovery percentage. Specimens deformed to 25% of extension showed sharp and better shape recoveries while heated above T_g and reported minimum recovery time. Almost equivalent recovery percentage of 10% deformed specimen was reported with a lengthy recovery time due to limited induced strain. It implies that during the stress-free strain's recoveries, the recovery time is remarkably influenced by the ultimate induced strain during shape programming.

In addition, the recovery time is directly linked to the end recovery temperature of low and high T_g transformations, heating rate, and the level of induced strains. Generally, at a higher end-recovery temperature and lower heating rate, the recovery time could be tenfold larger than the lower end-recovery temperatures at higher rates. Overall, the FFF printed SMPs thermomechanical cycle time was reduced up to 50 % then the IM produced and tested specimens. Moreover, both processes have their pros and cons, however, the tailored SMS properties are easy to control with few adjustments in printing and process parameters for the 3DP process than IM. In addition, critical objects prone to the ordered actuation for 4D printing following two-way and multiple-way SMS behaviors are limited to mold and removed using an injection molding process.

Furthermore, for future studies, morphological analysis through field emission scanning electron microscopy on SMPs produced by injection molding and additive manufacturing for 4D printing is recommended. For thriving thermomechanical tests with maximum shape memory properties, limited experimental time, and cost, the know-how of SMP behavior starting from the printing process to end recovery temperature is indispensable. AM process can drive maximum shape memory performance for complex and customized objects while the IM process is for simple and repetitive objects of similar functionalities. Thermomechanical cycle time is a critical parameter to investigate the quick repeatability of structure and multiple dynamic functionalities in time for 4D printing. The specific level of induced stress/strain driven by the deformation % in the elastic range can drive the SMS behavior for tailored applications of 4D printing.

Declaration of competing interest

The authors declare that they have no known competing financial interests or personal relationships that could have appeared to influence the work reported in this paper.

References

[1] O. Červinek, B. Werner, D. Koutný, O. Vaverka, L. Pantělejev, D. Paloušek, Computational approaches of quasi-static compression loading of SS316L lattice structures made by selective laser melting, Materials (Basel). 14 (2021). https://doi.org/10.3390/ma14092462.

[2] R. Fidel, Case study, AMable Europe, Prog Addit Manuf. 1 (2015) 9–20.

[3] L.X. Wang, D.F. Wang, L. Jiang, N. Bian, Q. Li, C.Y. Shen, Influence of process parameters on the morphologies of micro-injection molded polyformaldehyde parts, Int. Polym. Process. 34 (2019) 367–375. https://doi.org/10.3139/217.3776.

[4] I. Akbar, M. El Hadrouz, M. El Mansori, D. Lagoudas, Toward enabling manufacturing paradigm of 4D printing of Shape Memory Materials: Open literature review, Eur. Polym. J. 168 (2022) 111106. https://doi.org/10.1016/j.eurpolymj.2022.111106.

[5] E. Fuenmayor, M. Forde, A. V. Healy, D.M. Devine, J.G. Lyons, C. McConville, I. Major, Comparison of fused-filament fabrication to direct compression and injection molding in the manufacture of oral tablets, Int. J. Pharm. 558 (2019) 328–340. https://doi.org/10.1016/j.ijpharm.2019.01.013.

[6] B. Podsiadły, A. Skalski, W. Rozpiórski, M. Słoma, Are we able to print components as strong as injection molded?—comparing the properties of 3d printed and injection molded components made from abs thermoplastic, Appl. Sci. 11 (2021). https://doi.org/10.3390/app11156946.

[7] R.H.A. Haq, I. Taib, M.N.A. Rahman, H.F. Haw, H. Abdullah, S. Ahmad, A.M.T. Ariffin, M.F. Hassan, Mechanical properties of PCL/PLA Composite sample produced from 3D printer and injection molding, Int. J. Integr. Eng. 11 (2019) 102–108. https://doi.org/10.30880/ijie.2019.11.05.014.

[8] M. Franchetti, C. Kress, An economic analysis comparing the cost feasibility of replacing injection molding processes with emerging additive manufacturing techniques, Int. J. Adv. Manuf. Technol. 88 (2017) 2573–2579. https://doi.org/10.1007/s00170-016-8968-7.

[9] I. Akbar, M. El Hadrouz, M. El Mansori, D. Lagoudas, Continuum and subcontinuum simulation of FDM process for 4D printed shape memory polymers, J. Manuf. Process. 76 (2022) 335–348. https://doi.org/10.1016/j.jmapro.2022.02.028.

[10] Y. Zhao, Y. Chen, Y. Zhou, Novel mechanical models of tensile strength and elastic property of FDM AM PLA materials: Experimental and theoretical analyses, Mater. Des. 181 (2019) 108089. https://doi.org/10.1016/j.matdes.2019.108089.

[11] Y.Y.C. Choong, S. Maleksaeedi, H. Eng, S. Yu, J. Wei, P.C. Su, High speed 4D printing of shape memory polymers with nanosilica, Appl. Mater. Today. 18 (2020) 100515. https://doi.org/10.1016/j.apmt.2019.100515.

[12] Q. Zhang, T. Rudolph, A.J. Benitez, O.E.C. Gould, M. Behl, K. Kratz, A. Lendlein, Temperature-controlled reversible pore size change of electrospun fibrous shape-memory polymer actuator based meshes, Smart Mater. Struct. 28 (2019). https://doi.org/10.1088/1361-665X/ab10a1.

[13] M. Zare, M.P. Prabhakaran, N. Parvin, S. Ramakrishna, Thermally-induced two-way shape memory polymers: Mechanisms, structures, and applications, Chem. Eng. J. 374 (2019) 706–720. https://doi.org/10.1016/j.cej.2019.05.167.

[14] M. Aberoumand, K. Soltanmohammadi, E. Soleyman, D. Rahmatabadi, I. Ghasemi, M. Baniassadi, K. Abrinia, M. Baghani, A comprehensive experimental investigation on 4D printing of PET-G under bending, J. Mater. Res. Technol. 18 (2022) 2552–2569. https://doi.org/10.1016/j.jmrt.2022.03.121.

[15] S.T. Ly, J.Y. Kim, 4D printing – fused deposition modeling printing with thermal-responsive shape memory polymers, Int. J. Precis. Eng. Manuf. - Green Technol. 4 (2017) 267–272. https://doi.org/10.1007/s40684-017-0032-z.

[16] A. Kallel, M. Lamraoui, J. Fitoussi, A. Tcharkhtchi, The Residual Stress Effect on the Shape Memory Polymers, Residual Stress. 2016. 2 (2017) 151–156. https://doi.org/10.21741/9781945291173-26.

[17] S. Nam, E. Pei, The influence of shape changing behaviors from 4D printing through material extrusion print patterns and infill densities, Materials (Basel). 13 (2020). https://doi.org/10.3390/MA13173754.

[18] M. Mehrpouya, H. Vahabi, S. Janbaz, A. Darafsheh, T.R. Mazur, S. Ramakrishna, 4D printing of shape memory polylactic acid (PLA), Polymer (Guildf). 230 (2021) 124080. https://doi.org/10.1016/j.polymer.2021.124080.

[19] Y. Wang, X. Li, An accurate finite element approach for programming 4D-printed self-morphing structures produced by fused deposition modeling, Mech. Mater. 151 (2020) 103628. https://doi.org/10.1016/j.mechmat.2020.103628.

[20] T. Zhao, R. Yu, X. Li, B. Cheng, Y. Zhang, X. Yang, X. Zhao, Y. Zhao, W. Huang, 4D printing of shape memory polyurethane via stereolithography, Eur. Polym. J. 101 (2018) 120–126. https://doi.org/10.1016/j.eurpolymj.2018.02.021.

[21] J. Liu, Z. Chen, C. Hu, W. Yang, J. Wang, W. Xu, Y. Wang, C. Ruan, Y. Luo, Fluorescence visualization directly monitors microphase separation behavior of shape memory polyurethanes, Appl. Mater. Today. 23 (2021) 100986. https://doi.org/10.1016/j.apmt.2021.100986.

[22] W. Abuzaid, M. Alkhader, M. Omari, Experimental analysis of heterogeneous shape recovery in 4d printed honeycomb structures, Polym. Test. 68 (2018) 100–109. https://doi.org/10.1016/j.polymertesting.2018.03.050.

[23] M. Bodaghi, A. Serjouei, A. Zolfagharian, M. Fotouhi, H. Rahman, D. Durand, Reversible energy absorbing meta-sandwiches by FDM 4D printing, Int. J. Mech. Sci. 173 (2020) 105451. https://doi.org/10.1016/j.ijmecsci.2020.105451.

[24] H. Zeng, J. Leng, J. Gu, H. Sun, Modeling the thermomechanical behaviors of short fiber reinforced shape memory polymer composites, Int. J. Mech. Sci. 166 (2020). https://doi.org/10.1016/j.ijmecsci.2019.105212.

[25] No Title, Shape-Memory Behav. Therm. Stimul. Polyurethane Med. Appl. (2006). https://doi.org/DOI 10.1002/app.25567.

[26] F. Ira, Shape Memory Polymer Overall.pdf, n.d. http://www.smptechno.com/index_en.html.

[27] ASTM D638-14, ASTM D638-14, Standard Practice for Preparation of Metallographic Specimens, ASTM Int. 82 (2016) 1–15. https://doi.org/10.1520/D0638-14.1.

[28] B.L. VOLK, Three-Dimensional Modeling of Shape Memory Polymers Considering Finite Deformations and Heat Transfer, Statew. Agric. L. Use Baseline 2015. 1 (2015). https://oaktrust.library.tamu.edu/bitstream/handle/1969.1/148140/Volk, Brent.pdf?sequence=1.

[29] B.L. Volk, D.C. Lagoudas, Y.C. Chen, K.S. Whitley, Analysis of the finite deformation response of shape memory polymers: I. Thermomechanical characterization, Smart Mater. Struct. 19 (2010). https://doi.org/10.1088/0964-1726/19/7/075005.

[30] M.S. Germain, M.B. Alain, M.Q.I.H. Jerry, A holistic approach to design for 4D Printing, (2019).

[31] N. Tiwari, S.W. Gagare, A.A. Shaikh, Shape recovery analysis of the additive manufactured 3D smart surfaces through reverse engineering, Prog. Addit. Manuf. 6 (2021) 281–295. https://doi.org/10.1007/s40964-020-00162-2.

[32] D.J.M. G. Baer, T. S. Wilson, D. L. Matthews, Shape-Memory Behavior of Thermally Stimulated Polyurethane for Medical Applications, J. Appl. Polym. Sci. 103 (2006) 3882–3892. https://doi.org/10.1002/app.25567.

[33] M. Mohamadi, Interpretation of thermal transitions and phase transformations in semi-crystalline PVDF/PEO/graphene nanocomposites characterized by modulated-temperature DSC, J. Therm. Anal. Calorim. (2021). https://doi.org/10.1007/s10973-021-10997-8.

[34] R. Xiao, Modeling shape-memory effects in amorphous polymers, Mater. Today Proc. 16 (2019) 1462–1468. https://doi.org/10.1016/j.matpr.2019.05.324.

[35] X. Wang, H. Lu, X. Shi, K. Yu, Y.Q. Fu, A thermomechanical model of multi-shape memory effect for amorphous polymer with tunable segment compositions, Compos. Part B Eng. 160 (2019) 298–305. https://doi.org/10.1016/j.compositesb.2018.10.048.

[36] J. Li, Z. Liang, X. Zhang, Q. Kan, Experimental investigation on the thermo-mechanical deformation of thermo-induced shape memory polyurethane, Polymer (Guildf). 237 (2021) 124337. https://doi.org/10.1016/j.polymer.2021.124337.

[37] Y. Li, Z. Liu, A novel constitutive model of shape memory polymers combining phase transition and viscoelasticity, Polymer (Guildf). 143 (2018) 298–308. https://doi.org/10.1016/j.polymer.2018.04.026.

[38] W. Zhao, F. Zhang, J. Leng, Y. Liu, Personalized 4D printing of bioinspired tracheal scaffold concept based on magnetic stimulated shape memory composites, Compos. Sci. Technol. 184 (2019) 107866. https://doi.org/10.1016/j.compscitech.2019.107866.

[39] METTLER TOLEDO, Simultaneous Thermal Analysis, (2022). https://www.mt.com/int/en/home/products/Laboratory_Analytics_Browse/TA_Family_Browse/TGA_DSC/TGADSC3Plus_SF.html (accessed June 22, 2022).

[40] S. Ray, R.P. Cooney, Thermal degradation of polymer and polymer composites, Third Edit, Elsevier Inc., 2018. https://doi.org/10.1016/B978-0-323-52472-8.00009-5.

[41] M. Lei, K. Yu, H. Lu, H.J. Qi, Influence of structural relaxation on thermomechanical and shape memory performances of amorphous polymers, Polymer (Guildf). 109 (2017) 216–228. https://doi.org/10.1016/j.polymer.2016.12.047.

[42] J.E. Collins, H. Bell, Intelligent material, Tech. Proc. 2014 NSTI Nanotechnol. Conf. Expo, NSTI-Nanotech 2014. 2 (2014) 424–426. https://doi.org/10.1299/jsmemag.110.1060_156.

[43] A. Bakhtiyari, M. Baniasadi, M. Baghani, Development of a large strain formulation for multiple shape-memory-effect of polymers under bending, Int. J. Mech. Sci. 204 (2021) 106560. https://doi.org/10.1016/j.ijmecsci.2021.106560.

[44] H. Zhao, X. Lan, L. Liu, Y. Liu, J. Leng, Design and analysis of shockless smart releasing device

based on shape memory polymer composites, Compos. Struct. 223 (2019) 110958. https://doi.org/10.1016/j.compstruct.2019.110958.

[45] M.S. Irfan, S. Patel, R. Umer, M.A. Ali, Y. Dong, Thermal and morphological analysis of various 3D printed composite honeycomb cores, Compos. Struct. 290 (2022) 115517. https://doi.org/10.1016/j.compstruct.2022.115517.

[46] X. Wang, Y. Liu, H. Lu, N. Wu, D. Hui, Y.Q. Fu, A coupling model for cooperative dynamics in shape memory polymer undergoing multiple glass transitions and complex stress relaxations, Polymer (Guildf). 181 (2019) 121785. https://doi.org/10.1016/j.polymer.2019.121785.

Graphical Abstract